



**Australian Government**  
**Bureau of Meteorology**

**The Centre for Australian Weather and Climate Research**  
A partnership between CSIRO and the Bureau of Meteorology



# The CSIRO Mk3.5 Climate Model

Hal Gordon, Siobhan O'Farrell, Mark Collier, Martin Dix,  
Leon Rotstayn, Eva Kowalczyk, Tony Hirst and Ian Watterson

**CAWCR Technical Report No. 021**

May 2010



[www.cawcr.gov.au](http://www.cawcr.gov.au)





# The CSIRO Mk3.5 Climate Model

Hal Gordon, Siobhan O'Farrell, Mark Collier, Martin Dix,  
Leon Rotstayn, Eva Kowalczyk, Tony Hirst and Ian Watterson

*Centre for Australian Weather and Climate Research*

**CAWCR Technical Report No. 021**

April 2010

ISSN: 1836-019X

National Library of Australia Cataloguing-in-Publication entry

Title: The CSIRO Mk3.5 Climate Model [electronic resource] / Hal Gordon, Siobhan O'Farrell, Mark Collier, Martin Dix, Leon Rotstayn, Eva Kowalczyk, Tony Hirst and Ian Watterson.

ISBN: 978-1-921605-666 (PDF)

Series: CAWCR technical report; 21.

Notes: Bibliography.

Subjects: Climatic changes--Computer simulation--Greenhouse effect --Atmospheric circulation--Computer simulation

Dewey Number: 551.5253

Enquiries should be addressed to:  
Hal Gordon  
Centre for Australian Weather and Climate Research:  
A partnership between the Bureau of Meteorology and CSIRO  
GPO Box 1289 Melbourne  
Victoria 3001, Australia

Hal.Gordon@dar.csiro.au

## Copyright and Disclaimer

© 2010 CSIRO and the Bureau of Meteorology. To the extent permitted by law, all rights are reserved and no part of this publication covered by copyright may be reproduced or copied in any form or by any means except with the written permission of CSIRO and the Bureau of Meteorology.

CSIRO and the Bureau of Meteorology advise that the information contained in this publication comprises general statements based on scientific research. The reader is advised and needs to be aware that such information may be incomplete or unable to be used in any specific situation. No reliance or actions must therefore be made on that information without seeking prior expert professional, scientific and technical advice. To the extent permitted by law, CSIRO and the Bureau of Meteorology (including each of its employees and consultants) excludes all liability to any person for any consequences, including but not limited to all losses, damages, costs, expenses and any other compensation, arising directly or indirectly from using this publication (in part or in whole) and any information or material contained in it.

# Contents

<b>Abstract</b> .....	<b>1</b>
<b>1 Introduction and model history</b> .....	<b>3</b>
<b>2 Mk3 coupled model configuration</b> .....	<b>4</b>
2.1 AGCM .....	4
2.2 OGCM.....	4
<b>3 The Mk3.5 atmospheric model</b> .....	<b>4</b>
3.1 Atmospheric parameterizations .....	5
3.1.1 Radiation.....	5
3.1.2 Cloud microphysics.....	5
3.1.3 Semi-Lagrangian Transport of moisture/tracers and conservation.....	5
3.1.4 Surface drag .....	6
3.1.5 River routing scheme .....	6
3.1.6 Representation of effects of lakes in North America .....	6
3.1.7 Parameter changes for land surface scheme.....	6
3.2 Polar ice model .....	7
3.2.1 Ice advection.....	7
3.2.2 Ice-ocean velocities .....	7
3.2.3 Albedo of leads when freezing .....	7
3.2.4 Ice formation and redistribution.....	7
3.2.5 Treatment of ice break-off and ice melt at the ice perimeter .....	8
3.2.6 Ice parameters .....	8
3.2.7 Additional statistics .....	8
3.3 AGCM data for OGCM parameterizations.....	8
<b>4 The Mk3.5 ocean model</b> .....	<b>9</b>
4.1 Oceanic parameterizations .....	10
4.1.1 The Visbeck et al. (1997) specification of eddy transfer coefficients .....	10
4.1.2 Kraus-Turner mixed layer scheme .....	11
4.1.3 Horizontal mixing in specified locations.....	11
4.1.4 Horizontal mixing parameterized via the curl of surface stress .....	13
4.1.5 Horizontal mixing parameterized via diffusion in the upper ocean with magnitude of “Visbeck” coefficient in the interior.....	13
4.1.6 Tracer mixing to help link inland seas to world oceans .....	14
4.1.7 Drag in specific straits and bathymetry adjustments .....	15
4.2 OGCM data supplied to AGCM .....	16
<b>5 Coupling fields</b> .....	<b>17</b>
<b>6 Spin-up of the ocean and atmosphere</b> .....	<b>17</b>
<b>7 Initialization of the Mk3.5 coupled model</b> .....	<b>17</b>
<b>8 Coupled model climatology</b> .....	<b>18</b>

8.1	Skill scores.....	19
8.2	Global mean SST.....	20
8.3	Nino3.4.....	22
8.4	Modeled SST compared to observations .....	25
8.5	Global mean SSS .....	27
8.6	Modeled SSS compared to observations .....	28
8.7	Sea-ice volume .....	29
8.8	Surface water flux .....	32
8.9	Rainfall .....	34
8.10	Vertical mean ocean salinity .....	36
8.11	Stream function and overturning rates.....	37
8.12	Assessing changes in OGCM parameterizations.....	40
8.13	Surface fluxes before and after coupling.....	42
8.14	Antarctic surface fluxes.....	45
8.15	A key coupled model response.....	47
8.16	Concluding points .....	48
8.17	Data storage and access details.....	48
<b>9</b>	<b>Acknowledgements .....</b>	<b>49</b>
<b>10</b>	<b>References.....</b>	<b>50</b>
<b>11</b>	<b>Appendix.....</b>	<b>53</b>

## List of Figures

Fig. 1	10-year averaged Visbeck “vmhs” diffusivity ( $\text{cm}^2 / \text{sec} \cdot 10^{-6}$ ): February (left) and August (right). .....	10
Fig. 2	Mask for additional horizontal diffusion (value and location).....	12
Fig. 3a	Idealized mask showing typical land-sea boundary. ....	12
Fig. 3b	The generated “edge-mask” at the typical land-sea boundary.....	13
Fig. 4	North Sea - Baltic Sea grid points in the Mk3.5 (T63_2) ocean model. ....	14
Fig. 5	Mediterranean, Black Sea and Caspian Sea grid points in the Mk3.5 (T63_2) ocean model. ....	15
Fig. 6a	Torres Strait grid points in the Mk3.5 (T63_2) ocean model. ....	16
Fig. 6b	As Fig. 6a, except for Bering Strait.....	16
Fig. 7	The skill of models Mk3.0 and Mk3.5 in reproducing observational climatological means of various quantities (see text).....	19
Fig. 8	Global mean SST.....	20
Fig. 9	Mk3.5 global and hemispheric mean SST.....	21
Fig. 10	Mk3.5 global SST spectrum.....	22
Fig. 11a	Modeled Nino3.4 temperature anomaly. ....	23
Fig. 11b	Observed Nino3.4 temperature anomaly.....	23
Fig. 12	Nino3.4 temperature anomaly spectra (cpy = cycles per year: period in years given by $1/\text{cpy}$ ).....	24
Fig. 13	Composite of observed El-Nino events for years 1900-1999.....	24
Fig. 14	Composite of modeled El-Nino events for years 600-699.....	25
Fig. 15	Annual mean SST: Observations (upper) and Mk3.5 (lower). ....	25
Fig. 16a	Annual mean SST difference ( $^{\circ}\text{C}$ ): Coupled (451-500) minus Observations. ....	26
Fig. 16b	As Fig. 16a, except Coupled (years 1251-1300) minus Observations.....	26
Fig. 17	Global and hemispheric mean SSS.....	27
Fig. 18	Annual mean SSS: Observations (upper) and Mk3.5 years 451-500 (lower). ....	28
Fig. 19	Annual mean SSS difference (ppt): Coupled (1251-1300) minus observations. ....	28
Fig. 20	Change in Arctic Ocean river outflow rates ( $1000\text{m}^3 / \text{sec}$ shown by coloured boxes), and change in SSS (ppt shown by contours) by years 451-500. ....	29
Fig. 21	The coupled model NH and SH annual mean ice volume ( $10^3 \text{ km}^3$ ).....	30

Fig. 22	The SH ice thickness (m) for the AGCM spin-up and the Mk3.5 coupled run.....	31
Fig. 23	The NH ice thickness (m) for the AGCM spin-up and the Mk3.5 coupled run. ....	32
Fig. 24	Freshwater flux (in units of mm/day rainfall equivalent). ....	33
Fig. 25	Rainfall (mm/day): Observations (Xie and Arkin, 1997) and coupled model (years 1281-1300); December-February on left and June-August on right.....	34
Fig. 26	Annual precipitation (mm/day): Mk3.5 coupled model – Mk3.5 AGCM.....	35
Fig. 27	Global mean salinity per model level (50 year average): Ocean model spin-up and at end of coupled model run. ....	36
Fig. 28	Change in zonally averaged salinity: End of coupled run minus ocean model spin-up (50 year averages).....	36
Fig. 29	Ocean depth-integrated stream function (Sv) for (a) Mk3.0 ocean spin-up; (b) Mk3.5 ocean spin-up; (c) Mk3.0 coupled, y111-120; (d) Mk3.5 coupled, y111-120. ....	36
Fig. 30	Mean mixed layer depths in the Southern Ocean for Septembercalculated from Mk3.0 (upper panel) and Mk3.5 (lower panel) monthly density fields .The mixed layer depth was taken as the depth at which $\sigma_\theta$ first exceeded its surface value by more than $0.125 \text{ kg m}^{-3}$ . ....	38
Fig. 31	NH vertical-meridional streamfunction (Sverdrups): End of ocean spin-up (upper) and coupled model, years 1251-1300 (lower).....	39
Fig. 32	SH vertical-meridional streamfunction (Sverdrups): End of ocean spin-up (upper) and coupled model, years 1251-1300 (lower).....	40
Fig. 33	The zonal average surface water flux for Mk3.0 OGCM spin-up and Mk3.5# OGCM spin-up (# indicates no AGCM heat/salt fluxes). (Note: In Figs 32-40, the zonal average flux is calculated as the zonal integral of the flux divided by the zonal circumference at that latitude.).....	41
Fig. 34	As in Fig. 32 except for surface heat fluxes.....	42
Fig. 35	The surface water fluxes for stand-alone AGCM and OGCM. ....	43
Fig. 36	The surface heat fluxes for stand-alone AGCM and OGCM. ....	43
Fig. 37	The surface water flux for the Mk3.5 coupled model, together with stand-alone AGCM and OGCM fluxes.....	44
Fig. 38	The surface heat flux for the coupled model, together with stand-alone AGCM and OGCM fluxes.....	45
Fig. 39	Antarctic zonal surface water flux from the Mk3.0 and Mk3.5 models. ....	45
Fig. 40	Mk3.5 ocean precipitation and evaporation: Coupled model – AGCM.....	46
Fig. 41	Antarctic zonal net surface heat flux – Mk3.0 and Mk3.5 models. ....	47

Fig. 42	Topography pixels (x) used in W-E gradient calculation. ....	54
Fig. 43	Topography pixels (x) used in S-N gradient calculation. ....	55
Fig. 44	Schematic showing “pointer” locations at a trough point “T”. 1 = Easterly, 2 = North-Easterly, 3 = Northerly, etc. ....	57
Fig. 45	Schematic showing (i,j) locations of grid points representing the (T63) Great Lakes (L), together with (current model) “trough” indicator numbers. ....	59
Fig. 46	Amazon River monthly outflow rates. ....	61

## List of Tables

Table 1.	Level structure of the Mk3 OGCM and level depths.....	9
Table 2.	River outflows (1000m <sup>3</sup> sec <sup>-1</sup> ).....	35
Table 3.	River outflows (1000m <sup>3</sup> sec <sup>-1</sup> ).....	60



## **ABSTRACT**

This report contains a description of the CSIRO Mk3.5 Climate Model. The model is based on a prior model version (CSIRO Mk3.0). Significant changes were made to all parts of the model (atmosphere, land surface, ocean, and polar ice) with a view to reducing errors and climate drift in the Mk3.0 model. These changes are detailed herein. In particular, the ocean model (MOM2.2) has been upgraded to include spatially varying eddy transfer coefficients (Visbeck et al. 1997) and the Kraus-Turner (1967) mixed layer scheme.

Details about the Mk3.5 coupled model climatology are presented based on a 1300 year control simulation. The change in the global mean sea surface temperature over this period is only 0.2°C (a small warming), which is far superior to the behaviour of the prior model, which showed a much larger progressive cooling trend. The Mk3.5 also displays major improvement in oceanic behaviour in the high latitude Southern Ocean, where the stratification and circulation are generally much more realistic than in the prior model.

The “Mk3.5” version of the CSIRO climate system model is documented in this report. The Mk3.5 model has been developed from an earlier version (now designated as Mk3.0) which was documented in a prior Technical Report (Gordon et al. 2002). The report here gives details of the changes to the various component parts of the Mk3 model. Significant changes were made to all parts of the model (atmosphere, land surface, ocean, and polar ice) with a view to reducing errors and climate drift in the prior (Mk3.0) version of the model. The Mk3.5 coupled model has recently been used in a long control run (1300 years), and some details about the coupled model climatology are presented.



# 1 INTRODUCTION AND MODEL HISTORY

The history of climate model development within CSIRO has been documented in a recent publication (Smith, 2007). This publication gives an overview of the global climate modelling effort that has been underway, almost uninterrupted, since 1981. It also provides a comprehensive list of papers published by members of the CSIRO climate modelling team.

This Technical Report provides a description of the CSIRO climate model version designated Mk3.5, as used in the CMIP3 international model intercomparison project, with particular emphasis on the aspects changed since the Mk3.0 model version. The development of the Mk3.0 climate model (the forerunner to the Mk3.5 model described herein) has been detailed in a prior technical report, (Gordon et al. 2002). This is available on-line at

[http://www.cmar.csiro.au/e-print/open/gordon\\_2002a.pdf](http://www.cmar.csiro.au/e-print/open/gordon_2002a.pdf)

The Mk3.5 model has the same horizontal and vertical resolution as used in Mk3.0, but there have been some significant changes to model physical parameterization and the inclusion of representations of additional physical processes. The Mk3.5 model has been used in a long control run (1300 years) and for climate change experiments. Details of the model control run are included in this report.

In this report, a brief outline of the structure of the Mk3 climate model is given first (where “Mk3” henceforth is used to denote both the Mk3.0 and Mk3.5 model versions). The Mk3 model is a fully coupled ocean-atmosphere system, without the need for any adjustments of the interactive fluxes and component fields (for example, surface temperature) that couple the atmosphere to the oceans. The coupled model is in fact assembled from two major modules that are developed independently. These are denoted as the AGCM (the Atmospheric General Circulation Model), which contains the atmospheric, land surface, and sea-ice components, and the OGCM (the Ocean General Circulation Model). The initial phase of development resulted in the Mk3.0 coupled model. (Gordon et al. 2002). Simulations from the Mk3.0 model were contributed to the multi-model set used in the IPCC AR4 assessment (Randall et al., 2007). The second phase of development aimed to improve the coupled model climate simulation beyond that of the Mk3.0, by means of improved and/or extended physical parameterizations. This phase, lasting from about 2001 to 2005, resulted in the Mk3.5 model version.<sup>1</sup>

Section 3 of this report summarises the structure of the Mk3 coupled model. Sections 4 and 5 detail the changes made to the AGCM and OGCM, respectively, in going from the Mk3.0 to the Mk3.5 version. Sections 6-8 summarise changes in the coupling fields, in the separate model component spin-up procedure and in the initialization of the coupled model simulation. Details about the MK 3.5 coupled model performance in the control run are given in section 7. The Mk3.5 coupled model has been used in a control run of 1300 years, and details about model performance are given in section 7. The model has also been used in simulations of historical and future climate change, details of which will be reported elsewhere.

---

<sup>1</sup> There has been some further development of the atmospheric component since the Mk3.5 model was finalized. This has resulted in a model version designated as Mk3.6, with the major changes being the incorporation of an interactive aerosol treatment, and a new radiation package that allows for the direct effects of atmospheric aerosols to be included (Rotstayn et al., 2010).

## 2 MK3 COUPLED MODEL CONFIGURATION

An outline of the Mk3 model structure and resolution is now given. The model consists of the CSIRO spectral AGCM coupled to an ocean model (the GFDL MOM2.2 ocean model, Pacanowski 1996). As mentioned above, the AGCM has been developed as a unified package containing an atmospheric model, a land surface model, and a polar ice model. In the description of the AGCM and OGCM to follow, the horizontal grids used in the models are based around the “Gaussian” latitudes used in spectral models. These latitudes are not evenly spaced in the north-south (meridional) direction, although they are approximately so. Thus the meridional spacing quoted below will be approximate only. However, the longitudinal (east-west) spacing is regular.

### 2.1 AGCM

The Mk3 AGCM is a spectral model developed specifically to use horizontal spectral resolution T63 [1.875°EW x (approx.) 1.875°NS] with 18 vertical levels. This is also the AGCM resolution for the coupled Mk3 model. It is to be noted that the spectral model contains a Semi-Lagrangian Transport (SLT) method for the moisture components and atmospheric tracers such as aerosols. The number of grid boxes in the horizontal for the AGCM (T63) is 192 (EW) x 96 (NS) = 18,432. The vertical coordinate of the AGCM (18 levels) is a hybrid ( $\sigma : p$ ) vertical coordinate, where  $\sigma = p / p_s$ , with  $p$  being the vertical pressure and  $p_s$  the surface pressure.

### 2.2 OGCM

The ocean component for the Mk3 model is based on the GFDL MOM2.2 ocean model (Pacanowski 1996). It was configured with the specific aim of forming the coupled model with non-overlapping grid boxes when using T63 atmospheric resolution. However, the ocean model resolution is enhanced (relative to the AGCM) in the meridional direction in order that a more adequate representation of highly important El Niño features be obtained. The meridional resolution of the OGCM has thus been set at double that of the AGCM. The resolution is 1.875°EW x (approx.) 0.9375°NS (sometimes referred to as “T63\_2” resolution). This means that, horizontally, there are two ocean grid boxes to each atmospheric grid box in a coupled configuration. There are 31 vertical levels in the ocean model.

## 3 THE MK3.5 ATMOSPHERIC MODEL

The dynamical framework of the atmospheric model is based upon the spectral method with the equations cast in the flux form that conserves predicted variables (Gordon 1981). The atmospheric moisture variables (vapour, water and ice) are advected by a Semi-Lagrangian Transport (SLT) algorithm (McGregor 1993). There were no changes between Mk3.0 and Mk3.5 in the atmospheric model dynamical core. The Mk3.0 and Mk3.5 land surface schemes are essentially the same, except for the inclusion of a representation of the Great Lakes (see 4.1.6 below) and two parameter changes (4.1.7).

## 3.1 Atmospheric parameterizations

The physical parameterizations used in the atmospheric model were modified to some extent for the Mk3.5 model version. Some minor changes were made to help with, for example, improved conservation properties or more exact representation of certain processes. These will not be detailed here as the overall effects were minor in a climatological sense. Some of the more significant changes were as follows.

### 3.1.1 Radiation

The Mk3 model time-step is 15 minutes, and the radiation calculations are undertaken every 2 hours. The surface long-wave radiation is allowed to vary according to the varying surface temperature on a timestep by timestep basis. In the Mk3.5 model version, the computation of absorption by the atmosphere of the surface long-wave radiation between radiation steps has been improved. The effect has been to remove an unrealistic concentration of the variation in longwave forcing (due to the changing surface temperature between radiation steps) in the boundary layer, especially for clear skies. The main subroutines involved are *initfs*, *radh\_copy*, and *radh\_old*.

### 3.1.2 Cloud microphysics

The minor changes to the atmospheric and surface physical parameterizations described above altered the overall energy balance of the AGCM. Some small alterations to the cloud microphysics properties were made to achieve an annual mean energy balance at top-of-atmosphere.

### 3.1.3 Semi-Lagrangian Transport of moisture/tracers and conservation

The moisture/tracer variables are advected using a SLT scheme (McGregor, 1993). In the following discussion, the symbol  $(\tau)$  is used to denote values at the current timestep, while  $(\tau - 1)$  and  $(\tau + 1)$  are used to denote values at the previous and next timestep. The final moisture/tracer values (denoted by  $q$ ) after the advection leapfrog timestep,  $q(\tau + 1)$ , are compared with those before advection,  $q(\tau - 1)$ , to ensure that the mass-weighted (using surface pressure  $p_s$ ) global integral is conserved. A global *a posteriori* fixer is applied; the fixer also removes any negative moisture/tracer values created during advection. In the Mk3.0 model, the global mean (before and after) calculations used the same  $p_s(\tau)$  weighting (current timestep grid-point  $p_s$  values). The use of the current timestep  $p_s$  leads to a quite small, but unwanted non-conservation effect on a timestep by timestep basis. This has been rectified in the Mk3.5 model. In the Mk3.5 model the  $p_s$  weighting is now applied from data at the correct time. This requires that both  $p_s(\tau - 1)$  and  $p_s(\tau + 1)$  be available in grid point form. In the Mk3.5 atmospheric model time integration sequence, the spectral fields, including  $p_s$ , are time integrated before the SLT stage. Using the spectral  $p_s(\tau + 1)$ , a separate grid-transform is now undertaken to obtain  $p_s(\tau + 1)$  on the grid for use during the application of the SLT moisture transport algorithm which is carried out after the spectral time integration step. In computer modelling terms,  $p_s(\tau - 1)$ ,  $p_s(\tau)$ , and  $p_s(\tau + 1)$  are now retained in grid form using a rotating index to indicate time level. It is stressed that over a model year, the non-conservation

for moisture/tracers in the Mk3.0 model version was, in fact, very small due in part to the time-varying nature of the  $p_s$  field. The main subroutines involved are *gpst*, *pgrd*, *phys*, *dynm*, *assel*, *uvreal*, and *jmcgslt*. Of these, subroutines *gpst* and *pgrd* now undertake the transform of the spectral surface pressure to grid point space, with a rotating index for the three (3) time levels required (as set out above).

### 3.1.4 Surface drag

The surface drag in the Mk3.0 model for all surfaces (land, ocean, ice) was computed assuming a zero surface velocity. In the current coupled model (Mk3.5), the surface drag calculations now take into account the fact that the sea-ice and oceans have their own surface velocities. The sea-ice and ocean velocities are provided as running means before use in the surface drag calculations. This was incorporated to prevent unwanted leapfrog time-stepping interactions. For the AGCM in stand alone (non-coupled) mode, the ocean surface currents on a monthly basis come from ocean surface current data generated from the OGCM run in stand alone mode. The main subroutines involved are *ocicurr* and *atcurr*.

### 3.1.5 River routing scheme

At coastal points there can be runoff (river outflow) from the land. In the Mk3.0 model, runoff at inland grid points was transferred, without time delay, by a downslope method to appropriate coastal ocean grid points (subroutine *oldriv*). In the Mk3.5 model, this scheme has been enhanced whereby the runoff is transported from grid point to adjacent grid points (i.e. river flow) with appropriate computed downslope flow rates. This allows for a considerable time delay in some cases (e.g. the Amazon) between the time that the runoff occurs and the time that it arrives at the river mouth. Setting model option “newriver=T” implements this new river flow scheme. In addition, river outflows with large magnitude (such as the Amazon) being applied to the ocean model at isolated ocean grid points can lead to unwanted noise (a checker board patterns in the vicinity of the outflow). To help alleviate this, outflows larger than a critical value are effectively smoothed over a “river delta” before use by the ocean model. This smoothing is carried out in the AGCM (subroutines *spreadr*) before the data is supplied to the OGCM. More details about the new river routing scheme are supplied in Appendix A. The main subroutines involved are *newriv*, *landrun*, *datard*, *ocforce*, *surfa* and *surfb* (with implementation via logical variable “newriver”).

### 3.1.6 Representation of effects of lakes in North America

In the Mk3.5 model, appropriate land grid points are treated in a special manner that allows for the Great Lakes and other nearby large lakes to have a more realistic representation. These grid points are allowed to freeze and thaw. These lakes modify the rate of transfer of river water to the oceans (e.g. the St. Lawrence River). This parameterization of the lakes forms part of the “newriver” option, and details are also provided in Appendix A. The subroutines involved are as for the new river routing scheme set out above.

### 3.1.7 Parameter changes for land surface scheme

In the Mk3.5 model the soil density (dry) was set at 1600 Kg/m<sup>3</sup> for soil types 1-7 (See section “9” and “Table 3” in the Mk3.0 Technical Report – Gordon et al, 2002). It was 2600 Kg/m<sup>3</sup> in Mk3.0. In addition, the wilting content for peat was changed from 0.395 to 0.280 in Mk3.5.

## 3.2 Polar ice model

The sea-ice sub-component of the CSIRO coupled model is formulated as part of the AGCM. Details about the sea-ice model are given in O'Farrell (1998) and its application in O'Farrell et al. (1997) and O'Farrell and Connolley (1998). Since the Mk3.0 model version, there have been some minor changes to help with internal consistency and conservation aspects. There have also been some more significant changes as follows.

### 3.2.1 Ice advection

In the Mk3.5 model there has been some reworking of the sea-ice code to refine the "NCAR" ice advection algorithm at coastal points and at the ocean-ice edge (subroutine *advect*).

### 3.2.2 Ice-ocean velocities

The ocean velocities are now taken into account when computing the surface drag over oceans (see section 4.1.4 above). For consistency, the same approach is used for the ice at sea-ice points. At points with ice cover, the surface drag for the ice covered part takes the ice velocities into account (subroutine *atcurr* in conjunction with model option "*icevely=T*"). These velocities are applied as a running mean. In addition the ice velocities, which were filtered towards a slab motion for 2 latitude rows adjacent the North Pole in Mk3.0, are now Fourier filtered (subroutine *dynice*). Both the running mean and polar filter help to suppress the generation of noise in the ice velocities.

### 3.2.3 Albedo of leads when freezing

An additional improvement concerns the representation of surface albedo under freezing conditions for leads (open water part) at a grid point with (partial) ice cover. The albedo of the leads in Mk3.5 has been made dependent upon the rate of ice growth if model option "*icegrow=T*". The temperature in the leads is updated according to local heating/cooling rates (subroutine *surfupl*), and for ice generation conditions, the running mean of ice growth rate is formed. The ice growth rate is subsequently used (subroutine *surfice*) to modify the albedo of the leads and the apparent surface temperature of the leads. The leads are nominally assumed to have the albedo of sea water, with the surface temperature being that of the leads water. In Mk3.5, for freezing conditions, the rate of ice growth is used to modify the leads albedo towards a maximum of 0.3, and the leads surface temperature towards that of the surface temperature of the ice covered part of the grid (i.e. whiter and colder).

### 3.2.4 Ice formation and redistribution

In the Mk3.5 version of the sea-ice model there has been a change to the way that newly formed ice is used to update the ice thickness (and/or leads area) when the current ice at a grid point is thick ( $> 0.75\text{m}$ ). Sea-ice is formed when the temperature of leads water and water below old ice (at the same temperature) drops below a critical level. When the current ice at the grid point is thin ( $< 0.25\text{m}$ ), the newly formed ice is used to increase ice depth without changing the leads area. For thicker (current) ice conditions ( $> 0.25\text{m}$ ), the new ice is assumed to be moved laterally (wind blow) to add to the old ice (at its current thickness) with the leads area being reduced accordingly. In the case of the Mk3.5 model, a modification has been introduced when the current sea-ice depth exceeds  $0.75\text{m}$ . In this case, the newly formed ice in the leads area is also added to the current ice, but there is now a reduction in final average ice depth (old thick

ice + newly formed thin ice). There is also a correspondingly larger reduction in the final leads area. This modification forms part of a recoding of subroutine *surfupl* for the Mk3.5 model.

### 3.2.5 Treatment of ice break-off and ice melt at the ice perimeter

There has been an upgrade to the treatment of sea-ice that is deemed to have broken off near the edge of the polar ice. This is assumed to occur when ice advection at the ice edge causes a sub-critical amount of ice to be pushed into an adjacent ice-free grid point. This ice is now taken (in Mk3.5) to melt in the immediate vicinity of the ice-break off. This process then affects surrounding ice-free grid squares in an attempt to mimic ice movement on the ocean currents. The water flux and associated latent heat flux are distributed accordingly. See model subroutines *ocforce* and *icebreak1*. This is somewhat different to the Mk3.0 approach which allowed the ice break off to affect local oceans (North Atlantic, North Pacific, and Southern Ocean respectively) rather than local grid points (subroutine *icebreak*). The effect was spread equally over all ice free points poleward of a pre-specified latitude (i.e. the effect was spread out over each major ocean, rather than occurring in the immediate vicinity).

### 3.2.6 Ice parameters

The improved representation of leads conditions outlined above, and other improvements to the sea-ice code (e.g. the advection algorithm), has allowed for certain ice parameters used in each hemisphere (NH and SH) to be more consistently applied in Mk3.5. The minimum allowable leads fraction was set at 0.005 in the NH and 0.02 in the SH in Mk3.0. For Mk3.5, the minimum leads fraction is now set at 0.01 for both hemispheres. In addition there has been a change to the amount of heat flux from the ocean under the ice to the ice above (a “bottom” heat flux). This heat flux is, in part, a representation of unresolved passage of eddies under the ice resulting in the transfer of heat from the ocean to the ice. In the Mk3.0 model, the bottom heat flux, in  $Wm^{-2}$ , was set at 2 for the NH and 15 for the SH. In Mk3.5 (T63 resolution) the SH bottom heat flux has been reduced to 5 (subroutine *icecon*).

### 3.2.7 Additional statistics

The sea-ice model coding now produces a set of statistics (NetCDF files) about the processes (dynamic or thermodynamic) which control the changes in leads amount and changes in ice depth and extent. These have been particularly useful in determining the key processes that affect, for example, the evolution of polynyas in the model.

## 3.3 AGCM data for OGCM parameterizations

The OGCM in Mk3.5 now uses the GFDL MOM2 version of the Kraus-Turner (1967) mixed layer scheme (see section 5.1.2 below). This requires that the AGCM provide data for the  $(u^*)^3$  field ( $u^*$  is the frictional velocity from the surface drag calculations). It is provided as a running average. In addition, the Mk3.5 OGCM incorporates a parameterization of near surface horizontal mixing based on the curl of the surface stress. To obtain the curl of the stress in the AGCM, a transform to spectral space and subsequent inverse transform to grid space is carried out. The curl of the stress is also provided to the OGCM as a running mean. The subroutines involved are *ocntau*, *specstr* and *gridstr*.

## 4 THE MK3.5 OCEAN MODEL

The dynamical framework of the OGCM is based on the GFDL ocean model version MOM2.2. There were no changes between Mk3.0 and Mk3.5 ocean model dynamical core versions. In the following discussion of changes to the OGCM physical parameterizations, it will be useful to have the vertical structure of the Mk3 OGCM defined. The model levels are given in Table 1. There are 31 levels in the vertical, with the spacing of the levels gradually increasing with depth, from 10 *m* at the surface to 400 *m* in the deep ocean.

**Table 1. Level structure of the Mk3 OGCM and level depths.**

Model level k	Depth of layer ( <i>m</i> )	Layer thickness ( <i>m</i> )
1	5	10
2	15	11.62
3	28.25	13.51
4	42.02	15.71
5	59.66	18.26
6	78.54	21.22
7	102.11	24.67
8	127.88	28.68
9	159.47	33.34
10	194.56	38.75
11	236.97	45.04
12	284.65	52.36
13	341.69	60.87
14	406.38	70.75
15	483.19	82.24
16	570.87	95.83
17	674.86	111.45
18	793.76	129.61
19	934.08	150.73
20	1095.21	175.29
21	1284.65	203.85
22	1502.91	237.06
23	1758.77	275.69
24	2054.29	320.61
25	2400	372.85
26	2800	400
27	3200	400
28	3600	400
29	4000	400
30	4400	400
31	4800	400

## 4.1 Oceanic parameterizations

The physical parameterizations and options used in the ocean model were modified to some extent for the Mk3.5 model version. Briefly, the most significant changes are as follows.

- (1) Specification of spatially varying eddy transfer coefficients (Visbeck et al. 1997)
- (2) Inclusion of the Kraus-Turner (1967) mixed layer scheme
- (3) Horizontal mixing in specific locations (land-sea boundaries)
- (4) Horizontal mixing parameterization based on curl of surface stress
- (5) Horizontal mixing parameterization based on Visbeck coefficients
- (6) Tracer mixing to help link inland seas to world oceans
- (7) Drag in specific straits and bathymetry adjustments
- (8) Combined relaxation and coupled surface forcing during coupled model spin up

These are now discussed in more detail.

### 4.1.1 The Visbeck et al. (1997) specification of eddy transfer coefficients

The GFDL version of the Visbeck scheme was enabled in the Mk3.5 model. It was incorporated as parallelized code, and is activated by the “IFDEF” compilation option “vmhs\_diffusivity”. It allows for a parametric representation of oceanic geostrophic eddy transfer of heat and salt coefficients that vary in space and time in a manner that depends on the large-scale density fields. The Visbeck scheme operates over model levels 7 to 19 only. The MOM3 version of the Visbeck scheme was transferred into the MOM2.2 code (subroutine *nonconstantdiff.F*) and the subroutine *isopyc.F* was adapted to mesh in the relevant additional calls. Some of the coefficients used in the Visbeck scheme were modified to better fit the length scales and resolution in the current model.

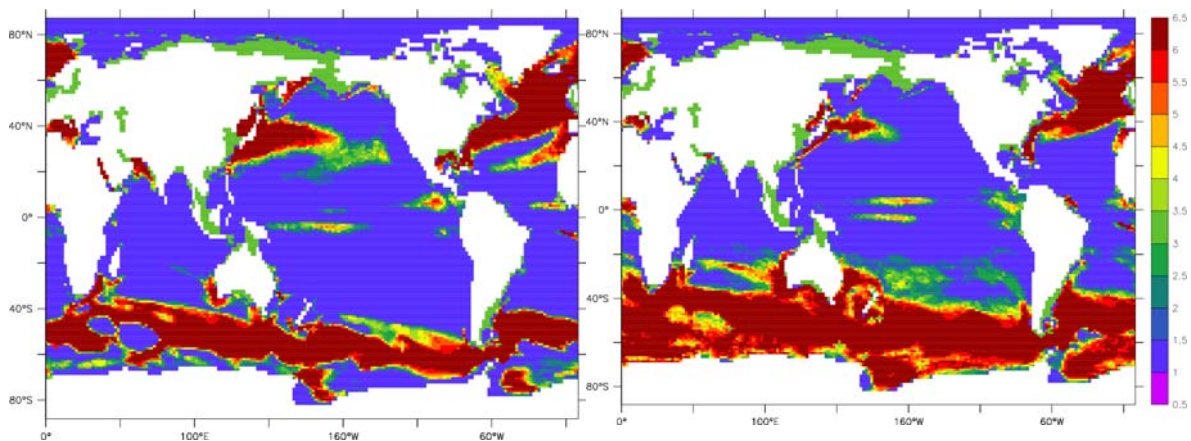


**Fig. 1** 10-year averaged Visbeck “vmhs” diffusivity ( $\text{cm}^2 / \text{sec} \cdot 10^{-6}$ ): February (left) and August (right).

Figure 1 shows an example of the modeled spatial distribution of the “vmhs” diffusivity in the Visbeck scheme, where the highest values are in the Southern ocean, in the tropics and in the Gulf Stream and Kurishio. The spatial pattern, with higher values in the Southern Ocean, improves the ability of the model to represent the correct stratification whilst still allowing convection in the Labrador and Greenland Seas to feed into the North Atlantic meridional thermohaline circulation.

### 4.1.2 Kraus-Turner mixed layer scheme

The Kraus-Turner mixed layer parameterization is employed in the Mk3.5 model. It is based upon the FLAME configuration (Family of Linked Atlantic Model Experiments – Dengg et al., 1999) of the GFDL MOM2.1 ocean model code. This is activated by the “IFDEF” compilation option “ktmix”. The formulation used includes the wind-driven part only, in conjunction with the ‘Sterl and Kattenberg’ numerical scheme. The Kraus-Turner module was implemented as parallelized code in the Mk3.5 model. It was found that the code had to be reworked to implement the change in mixed layer depth as a tendency calculation, rather than a direct update, in order to help with numerical stability.

### 4.1.3 Horizontal mixing in specified locations

The tracer code allows for additional horizontal diffusion for specific locations (both Mk3.0 and Mk3.5). This helps to prevent the (possible) generation of negative salinities in coupled mode. It also helps to alleviate warm/cold spots in some narrow (1 grid point wide) bays and straits. This extra horizontal mixing is activated via the use of the “IFDEF” compilation option “ghdiff” (Globally-variable Horizontal DIFFusion). The grid points at which additional horizontal diffusion is imposed are obtained from a global mask “ghd-mask”. The coding for this diffusion has been simplified somewhat in the Mk3.5 version of the OGCM, and the specifications within the global mask altered to some degree. This mask is specified through an input file “maskghd.t63\_2” in the Mk3.5 model. This is illustrated in the Fig.2. This mask (ocean points) shows integer values of  $mm = 0$  (blue - no additional diffusion for the majority of points),  $mm = 2$  (green) or  $mm = 4$  (yellow) for some specific regions. The amount of diffusion is defined by  $Ahx * mm$  for  $mm > 0$  with  $Ahx = 10^7 \text{ cm}^2 / \text{sec}$ .

The regions shown in the map for additional diffusion were specified to help achieve the following objectives. The first objective is to link ocean grid points having no velocity vectors (e.g. 1 grid point wide channels) or poor connectivity to the major oceans (e.g. Canadian-Arctic region). In the Antarctic, some additional tracer diffusion was specified in the Ross and Weddell Seas. Here there are significant annual variations in heat and salt flux due to sea-ice formation and melting which are in relatively confined areas. This additional diffusion (defined via the mask) is allowed to operate over model levels 1 to 12 (surface to ~285m, and is then phased out linearly by level 15 (~483 m).

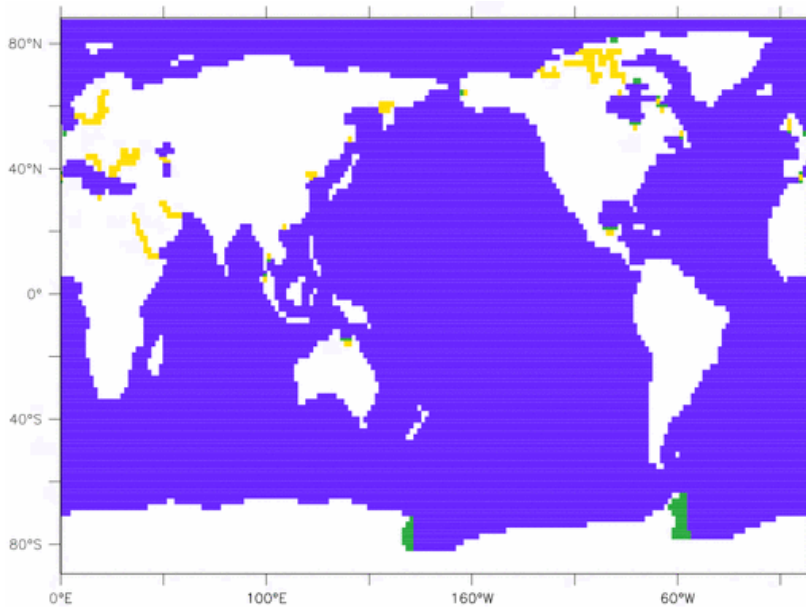


**Fig. 2 Mask for additional horizontal diffusion (value and location).**

In the Mk3.5 model, an additional way of specifying horizontal diffusion of tracers has been incorporated in the vicinity of land-sea boundaries. At the land-sea boundary it has been found in the stand alone ocean model runs, as well as in coupled model runs, that there is a tendency for some horizontal inhomogeneity in the model tracer fields. This is partly due to the step-like nature of the grid on irregular coastlines, with velocity vectors being at the corners of tracer grid points and velocities being zero on the “coast”. In addition, there are strong inflows from rivers at some coastal points, and the ocean model can tend to suffer from these isolated strong fresh water inflows (see also comments in AGCM description, section 4.1.5 above). Thus to help smooth the tracer solution in these coastal regions, an “edge-mask” for the model is computed. This edge-mask allows for additional horizontal mixing at the two grid boxes next to the land boundary. This edge-mask computation, carried out by the model code, derives values of 2 for ocean grid points next to land, values of 1 for the next seaward point, otherwise 0 for other sea points. An idealized sample grid mask for a coastal region is shown diagrammatically in Fig. 3a (“.”= Land and “s”=Sea).

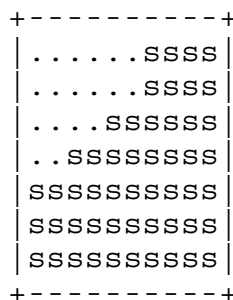


**Fig. 3a Idealized mask showing typical land-sea boundary.**

A mask (edge-mask) is formed with integer values “*me*” = 0, 1, or 2 for sea points as illustrated in Fig. 3b:

```

+-----+
| .....2100 |
| .....2100 |
| ....222100 |
| ..22211100 |
| 2221110000 |
| 1111000000 |
| 0000000000 |
+-----+

```

**Fig. 3b** The generated “edge-mask” at the typical land-sea boundary.

The land points (“.”) are not active with regard to this mask. The amount of horizontal diffusion for sea points is defined by  $Ahx * me$ , and operates over levels 1 to 6 of the current model (i.e. levels above that defined for the Visbeck scheme). Note that the extra diffusion defined by “ghd-mask” and that defined by “edge-mask” above are not added, but selected by choosing the maximum value from either method.

#### 4.1.4 Horizontal mixing parameterized via the curl of surface stress

This particular parameterization has been included to help represent the unresolved horizontal mixing due to wind driven horizontal mixing by the passage of large and small scale atmospheric eddies. This has been implemented by computing the curl of the surface stress generated by the atmospheric model (via a spectral transform procedure in the AGCM). The OGCM horizontal mixing amount  $Ahstr$  (dynes/cm\*\*2) is made proportional to the AGCM generated curl of the surface stress “*curlstr*” (N/m):

$$Ahstr = curlstr * 10^6$$

The *curlstr* generated by the AGCM is provided as a running average for use in the OGCM parameterization. It is applied to the top 6 levels of the ocean, and decreases with depth (ratios 1, 1, 0.8, 0.6, 0.4, 0.2). This extra horizontal mixing is added to the mixing computed by maximum of (5.1.2) and (5.1.3) above.

#### 4.1.5 Horizontal mixing parameterized via diffusion in the upper ocean with magnitude of “Visbeck” coefficient in the interior

The Visbeck and GM schemes (specification of eddy transfer coefficients) taper off into the mixed layer using one of two formulas. The Mk3.5 system uses the “gkw\_taper” option. When it was clear that additional mixing was needed in the mixed layer before the implementation of the curl of the wind stress scheme was invoked (section 5.1.4), the value calculated by the taper scheme was implemented as a horizontal diffusion in the top 12 model layers. The amplitude of the horizontal diffusion is the variable Gent McWilliams value calculated by the Visbeck scheme which represents the eddy mixing in the ocean, weighted by the taper value for this depth interval. This parameterization of horizontal mixing in the ocean model is invoked when the “IFDEF” compilation option “mixed\_layer\_horizontal” is turned on. This horizontal mixing is added to the mixings outlined above (see end of 5.1.4)

#### 4.1.6 Tracer mixing to help link inland seas to world oceans

The Baltic Sea is much less saline than the world oceans in reality and in the model. This is brought about by the river inflows around the edge of the Baltic Sea, together with connectivity to the world oceans being restricted in the Denmark region. To help prevent the water in the Baltic in the model from becoming too fresh, some “across-land” mixing has been included. The mask in Fig. 4 shows the points affected by this mixing (denoted by letters “**W**” and “**E**”):

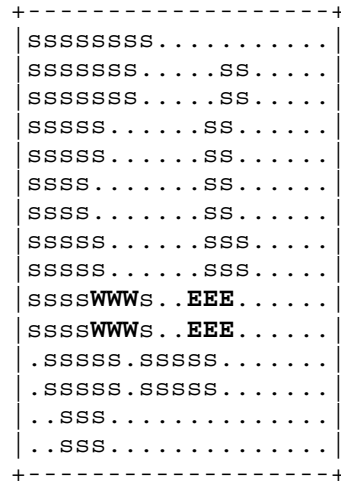


Fig. 4 North Sea - Baltic Sea grid points in the Mk3.5 (T63\_2) ocean model.

The model salinity is expressed in terms of the ocean model tracer variable “*Sal*” where

$$Sal = (S - 35) / 1000$$

and *S* is the salinity in ppt. The across-land mixing, if any, takes place per latitude row. It is invoked only when the average of the salinity *S* for the “**E**” points (in the Baltic) in the row is less than 9 ppt, i.e.  $Sal < -0.026$ . The mixing is then computed by adding/subtracting the quantity “ $\Delta Sal$ ” to **E**/**W** points. The value of  $\Delta Sal$  is given by

$$\Delta Sal = 7.2 * 10^8 * \Delta t^{TS} * (Sal(W) - Sal(E))$$

in which  $Sal(W)$  and  $Sal(E)$  are the average of the *Sal* values for the three **W** and **E** points in the latitude rows. The quantity  $\Delta t^{TS}$  is the timestep for the model tracers (Temperature and Salinity). The salinity mixing takes place for the upper six model levels only.

There is also similar across-land mixing of salinity for the Caspian and Black Seas included in the Mk3.5 model. This is because the Caspian Sea is not linked in the model to the rest of world oceans. Thus a non-zero annual mean fresh-water-flux for the Caspian Sea may lead to unrealistic changes in mean salinity for coupled model runs spanning many centuries. Shown in Fig. 5 is the grid-point mask for the Mediterranean, Black Sea, and Caspian Sea regions in the Mk3 model. The salinity of the Caspian Sea points denoted by “**E**” are of a similar magnitude to those points in the Baltic Sea denoted by “**W**”. In the model, the salinity of these **E** and **W** points are mixed in the same way as for the Baltic Sea mixing described above, but there is no restriction on the Caspian Sea salinity for the **E** points (i.e. across-land mixing takes place continuously).





## 5 COUPLING FIELDS

The surface stress related terms coupling the AGCM and the OGCM have been modified in the Mk3.5 model. In the Mk3.0 model the surface drag was calculated as part of the AGCM surface flux calculations, and assumed a zero surface velocity (both ocean and sea-ice velocities set to zero). In the Mk3.5 model, the ice velocities are now used for ice covered points, with a running mean applied. Similarly, at ocean points, the ocean velocities are passed to the AGCM (coupled mode) for the surface drag calculation. The surface stresses so calculated, together with  $(u^*)^3$  (where  $u^*$  is the friction velocity), are subjected to a running mean before use by the OGCM. This help with suppressing leapfrog two-step noise between the models, especially near the poles.

## 6 SPIN-UP OF THE OCEAN AND ATMOSPHERE

The spin up method used prior to initiation of the Mk3.5 coupled model integrations is similar to that used in the Mk3.0 model. The AGCM, which consists of atmospheric, land-surface, and sea-ice components, is spun up during the development phases, culminating in a 10-year run prior to coupling. It uses an annual cycle of observed SSTs, and has ocean currents (taken from a prior ocean model spin-up) provided for use by the sea-ice sub-component and in the surface drag calculations. The AGCM time-step during spin up is 15 minutes.

The oceanic component (Mk3.5 version) is spun up for the order of 1000 years in a configuration identical to that to be employed in the coupled model integration. The spin-up uses the technique of asynchronous time stepping (Bryan 1984), where tracer time steps are much larger (0.5 day) than momentum time steps (15 minutes). Modest discrepancies may occur in the seasonal cycling of the ocean under this time-step regime (Bryan 1984). Hence an additional several years of integration are conducted as a final stage of the oceanic spin-up, where the time steps are set to be 15 minutes for all prognostic model variables, which is the same as that used in the coupled model integration.

During spin-up, the oceanic component is forced by the annual cycle of wind stress, heat fluxes and freshwater flux, as derived from the spin-up simulation of the stand-alone atmospheric model. It is also forced at the surface by a relaxation of surface temperature and salinity to observed climatology (6 day and 200 day damping times respectively). AGCM heat and water fluxes were not used in the Mk3.0 ocean model spin-up.

## 7 INITIALIZATION OF THE MK3.5 COUPLED MODEL

The Mk3 coupled model is generated by combining the compiled code for both AGCM and OGCM, and by using the master routine (*main*) to control the sequence of events. (A “flux coupler” is not required). The sequence of subroutine calls for both the AGCM and OGCM have been set out in the Mk3.0 Technical Report (Gordon et al., 2002). The formulation of the surface fluxes (momentum, heat and water) is given in that report. In particular, the fluxes in the presence of partial sea-ice cover and partial open water (leads) at a grid point is also detailed. As was the case in Mk3.0, flux adjustments are not used in the Mk3.5 model.

In order to initialize the Mk3.0 coupled model, the AGCM and OGCM components were simply combined, and the coupled model started from the final restart files of the spin-up AGCM and GCM runs. Clearly, there is no feedback between ocean and atmosphere during

spin ups, and it is to be expected that such a coupled model will experience some initial adjustment phase, and some climate drift, as the various feedbacks between ocean and atmosphere come into play. This was evident in the global mean cooling during the first 80 years of the Mk3.0 couple model run - see “Fig.7” and the associated discussion in the Mk3.0 technical report (Gordon et al., 2002). The cooling in the Mk3.0 coupled run is also shown in Fig.8 below. As discussed in Mk3.0 report, there are other possible ways of initiating a coupled model from the spun-up AGCM and OGCM components. In the Mk3.5 version, the coupled model code has been modified to allow for the relaxation of the ocean surface temperature and salinity back to observations (as used in the oceanic spin up) whilst being driven by the momentum, heat and water fluxes at the surface. The use of surface relaxation during the initial years of the Mk3.5 coupled model run helps to reduce the “coupling shock”. The relaxation is only employed over the first 5 years of the model run, and the strength of relaxation is reduced year by year for temperature - the damping times are 20,30,40,60,80 days for years 1,2,3,4,5 respectively, compared to 6 days during spin-up. The damping time for salinity during this period remained at 200 days (the same as during spin-up).

## 8 COUPLED MODEL CLIMATOLOGY

To give an indication of the performance of the Mk3.5 coupled model, an outline of the climatology obtained during a long period integration of the model is now presented. At the time of this report, more than 1300 model years have been completed in the control run. Data from the control run is available for general analysis and details about accessing the data is given in subsection 9.17. In the subsections below the following topics are covered:

- 9.1 Skill scores
- 9.2 Global mean SST
- 9.3 Nino 3.4
- 9.4 Modeled SST compared to observations
- 9.5 Global mean SSS
- 9.6 Modeled SSS compared to observations
- 9.7 Sea-ice volume
- 9.8 Surface water flux
- 9.9 Rainfall
- 9.10 Vertical mean ocean salinity
- 9.11 Ocean stream function and overturning rates
- 9.12 Assessing changes in OGCM parameterizations
- 9.13 Surface fluxes before and after coupling
- 9.14 Antarctic surface fluxes
- 9.15 A key coupled model response
- 9.16 Concluding points
- 9.17 Data storage and access details

Most sections address the stability of the coupled model and properties of the oceanic control simulation, which were a focus of the development of the Mk3.5 coupled model from the earlier Mk3.0 version. The skill of the model in simulating the atmospheric and surface climate is, of course, crucial, and a comparison of the performance of both model versions is now presented.

## 8.1 Skill scores

Many aspects of climate may be important to particular applications. For instance in the recent report ‘Climate Change in Australia’ (CSIRO, 2007) CMIP3 simulations, including those from Mk3.0 and Mk3.5 were assessed on their seasonal averages of surface temperature, rainfall and sea level pressure in the Australian region. Our presentation here is limited to skill scores that provide a single overall evaluation of global climatological fields. We consider a range of quantities, including some that important to climate applications, some that relate to hydrological and radiative processes and others are important to the response of a model to imposed climate forcing. Such an evaluation was used in assessing the Mk3.0 atmospheric model by Watterson and Dix (2005). As discussed by Randall et al. (2007), comparison of a coupled model control simulation with observations from recent decades is complicated by the climate forcing that has occurred. We follow them in testing the standard climatological period, 1961-1990, taken from the twentieth century (or 20C3M) simulations of our models submitted to CMIP3 (see section 9.17).

For each of 13 quantities and each of the four seasons, the global field from a model is compared to the best available observational field ‘Obs-1’ using the non-dimensional statistic  $M$ , as defined in the caption. The average of the four seasonal scores is shown in the histogram in Fig. 7, with the bar representing the value for Mk3.5 shown to the right of that for Mk3.0, in each case. A value of 1 for  $M$  indicates perfect agreement, while 0 indicates no skill. As can be seen both models produce considerable skill in each quantity. The contribution of the global mean bias to the disagreement is indicated by bars coming down. In many cases this is rather small.

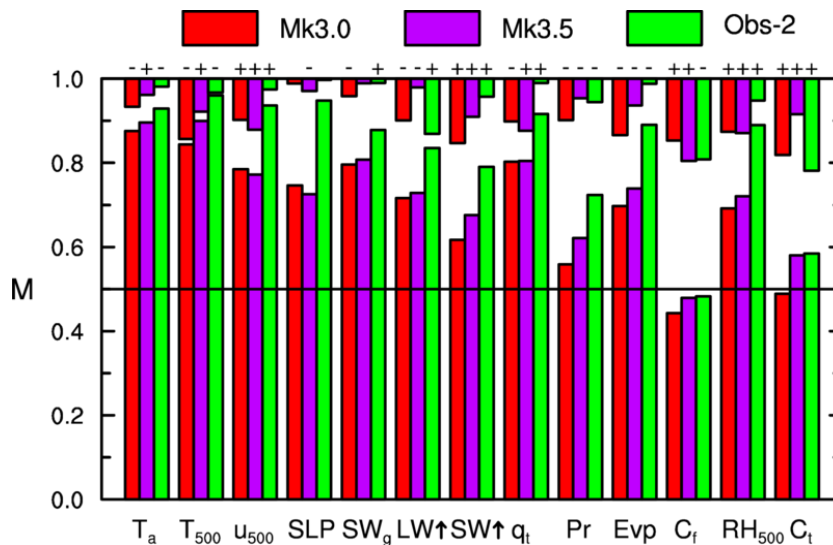


**Fig. 7** The skill of models Mk3.0 and Mk3.5 in reproducing observational climatological means of various quantities. The third score indicates the agreement between a second observation data field (Obs-2). Bars up from 0 give  $M$  scores for the global domain, where  $M = (2/\pi) \arcsin[1 - \text{mse} / (\text{VX} + \text{VY} + (\text{GX} - \text{GY})^2)]$ , with mse the mean square error between the model field  $X$  and observed field  $Y$ , and  $V$  and  $G$  are variance and regional mean of the fields (as subscripted). The bars down from 1 give  $M$  scores when the magnitude of the global mean bias is used in place of mse. Both are averaged over the results for DJF, MAM, JJA and SON. A + or – symbol indicates the sign of the mean bias, if this is the same in all four seasons.

In practice, there is considerable uncertainty in the true climatology of each field. In addition, some apparent error must occur due to the effect of unforced variability on averages over 30-years. To provide a comparison, a second observational field ‘Obs-2’ is compared with the first and the M score shown as a third set of bars.

The choice of observational data for comparison is complicated by their varying quality over time and location. The forced response since 1990 is likely to be less than the improvement in quality in recent decades, compared to earlier ones, so using data from outside the 1961-1990 period can be justified. For global atmospheric fields, daily ‘re-analysis’ data available from several major forecasting centres is preferred. We use here the recent ERA-interim data set (Simmons et al., 2009), averaging data over the 20 years 1989-2008. This is taken as Obs-1 for the 10 quantities (as labelled in Fig. 7)  $T_a$  = Air (2m) temperature;  $T_{500}, u_{500}$  = 500mb temperature, zonal velocity;  $SLP$  = Sea level pressure;  $SW_g$  = Short wave at ground;  $q_t$  = Total atmospheric water;  $P_r$  = Precipitation;  $EvP$  = Evaporation;  $RH_{500}$  = 500mb relative humidity; and  $C_t$  = Cloud (total) fraction. For the top-of-atmosphere quantities  $LW_{\uparrow}, SW_{\uparrow}$  Upward long, short wave radiation, and  $C_f$  = Cloud forcing; Pincus et al. (2009) have provided a climatology based on CERES satellite data over 2000-2005, used as Obs-1. The Obs-2 fields are the GPCPv2.1 precipitation data over 1979-2008 (updated from Adler et al. 2003), the CRU surface temperatures for 1961-1990 (but on a 5 degree grid), and from NCAR, the satellite-based NVAP data set over 1988-1999 for  $q_t$  and ISCCP cloud and surface radiation data over 1983-2004. In some cases extrapolation over missing data is used. Other fields are from the ERA40 re-analyses over 1957-2002 (which is not fully independent of ERA-interim, of course).

As can be seen, the uncertainties in the climatological fields for precipitation, cloud forcing and total cloud appear large. In this respect, the model scores are not so poor. Of course, some other fields have their spatial variation strongly controlled by incoming solar radiation, which is specified.

As mentioned in section 4, many of the changes to the AGCM and the polar ice model between versions Mk3.0 and Mk3.5 were not expected to have a major impact on the model climatology. However, there was an improvement in skill in the Mk3.5 model relative to the Mk3.0 model in 11 out of the 13 quantities shown. The average M for Mk3.0 is 0.697, and for Mk3.5 it is 0.727. This is a useful improvement, particularly when the average for Obs-2 is 0.828.

## 8.2 Global mean SST

The Mk3.5 model has been found to have only a small amount of drift in global mean SST during the 1300 year control run<sup>2</sup>. In contrast, the Mk3.0 model had a cooling trend in its 500 year control run. The global mean SST for both models for the first 500 years is shown in Fig. 8. The data in this figure has been smoothed with a 10 year running mean. The Mk3.5 model clearly has little drift in this period, compared to about a 1.5°C cooling in Mk3.0. Thus the

---

<sup>2</sup> A model physics change was made at end of year 80 in the Mk3.5 control simulation; with the re-activation of the bulk Richardson number mixing scheme of Price et al. (1986). This scheme was used in the Mk3.0 simulations. Its neglect in the early Mk3.5 control simulation was associated with an overly active and periodic ENSO, apparently related to an inadequate level of near surface mixing in the tropics associated with shear in the water column. The use of the output from this first 80 years in analysis is not recommended, and we only include this period in some time series plots for completeness.

changes to the model physical parameterizations have made the Mk3.5 model more stable with regard to global mean temperature.

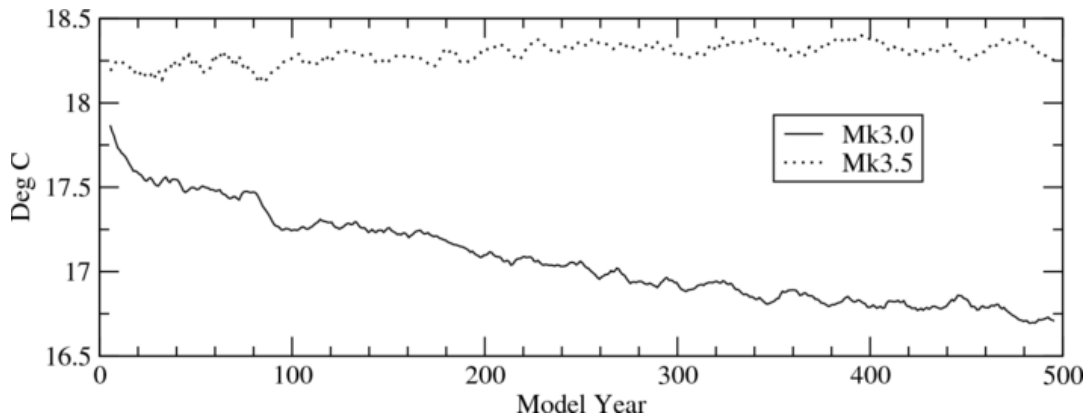


**Fig. 8 Global mean SST.**

The change in the Mk3.5 global mean SST for the entire control run (1300 years) is shown in Fig. 9 (10 year running means). The change in the global mean SST over the 1300 years is about  $0.2^{\circ}\text{C}$  (a small warming). The changes in the hemispheric mean SST are also shown in this figure. The SH showed an initial cooling trend (to about year 200) and then a warming trend. At the end of 1300 years the mean temperature for the SH was only a little warmer than at the start of the run. The NH, on the other hand displayed larger changes. Over the first 200 years the NH warmed by about  $0.6^{\circ}\text{C}$ , which was followed by a very slight cooling for the remainder. The NH mean temperature at the end of 1300 years was about  $0.4^{\circ}\text{C}$  warmer than at the start. Thus it appears that there is an adjustment phase (about 200 years) in which the model hemisphere mean temperatures move in opposite directions, followed by a slower recovery phase.

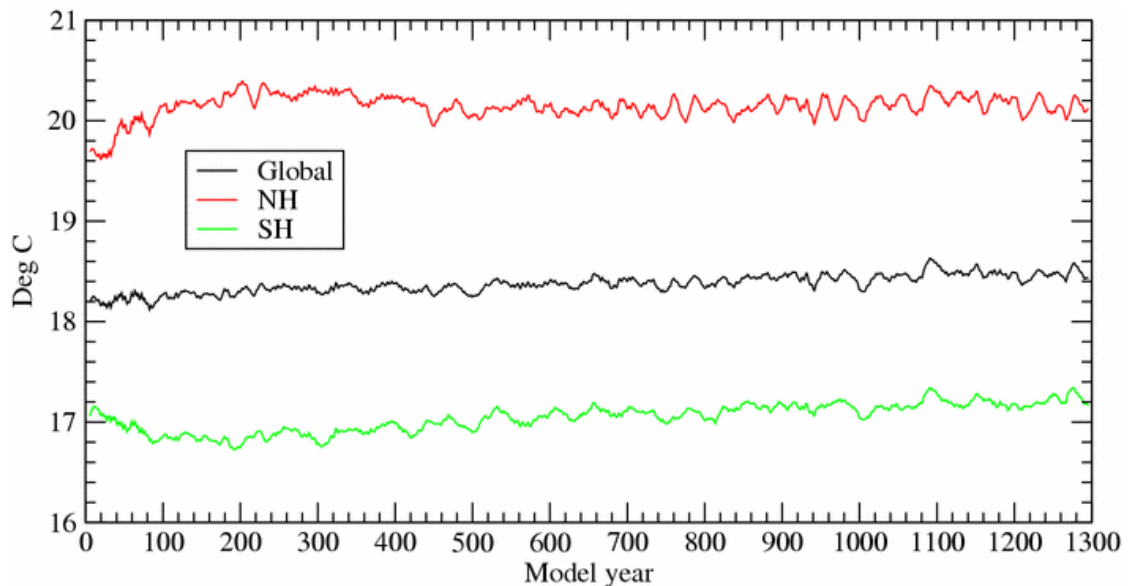


**Fig. 9 Mk3.5 global and hemispheric mean SST**

A time series analysis of the annual (unsmoothed) variations in the global mean temperature was undertaken. This was carried out for de-trended data from years 501 to 1300. The spectrum is shown in Fig. 10.

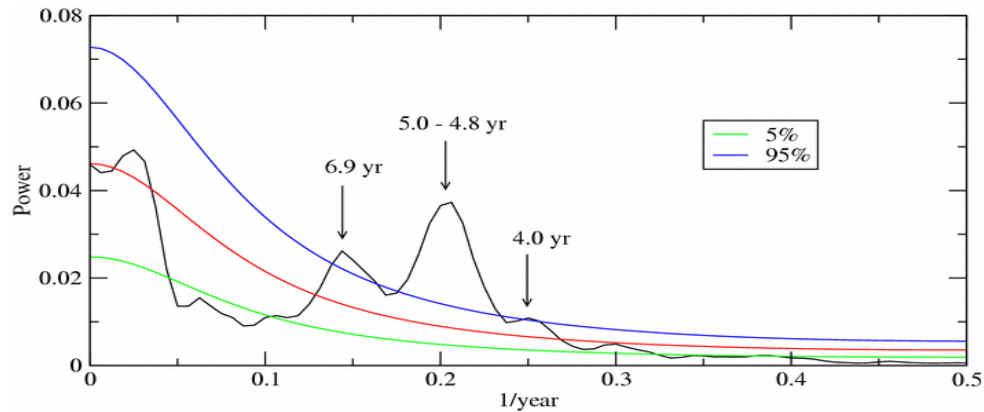


**Fig. 10 Mk3.5 global SST spectrum.**

The spectrum shows that there are significant peaks (95% confidence level) at about 6.9, 4.9 and 4 years. A similar analysis of data for the NH and SH over the same period shows significant peaks at 6.9 and 5 years for the NH, and significant peaks at 6.9, 4.8, and 4 years for the SH. Thus the global spectral response covers the range for both hemispheres.

### 8.3 Nino3.4

The SST response in the Pacific has a fairly realistic El Nino/La Nina structure (see later description). The time series analysis for the SST anomaly in the “Nino3.4” area in the Pacific (170W:120W, 5N:5S) for years 501 to 1300 (see Fig. 11a below) is quite similar to that of the global SST anomaly. This indicates the dominance of the Pacific SST anomaly in the global mean SST anomaly spectrum. The Nino3.4 SST anomaly for years 501 to 1300 is displayed in the Fig. 11a. Also included is an expanded section for years 600 to 700.

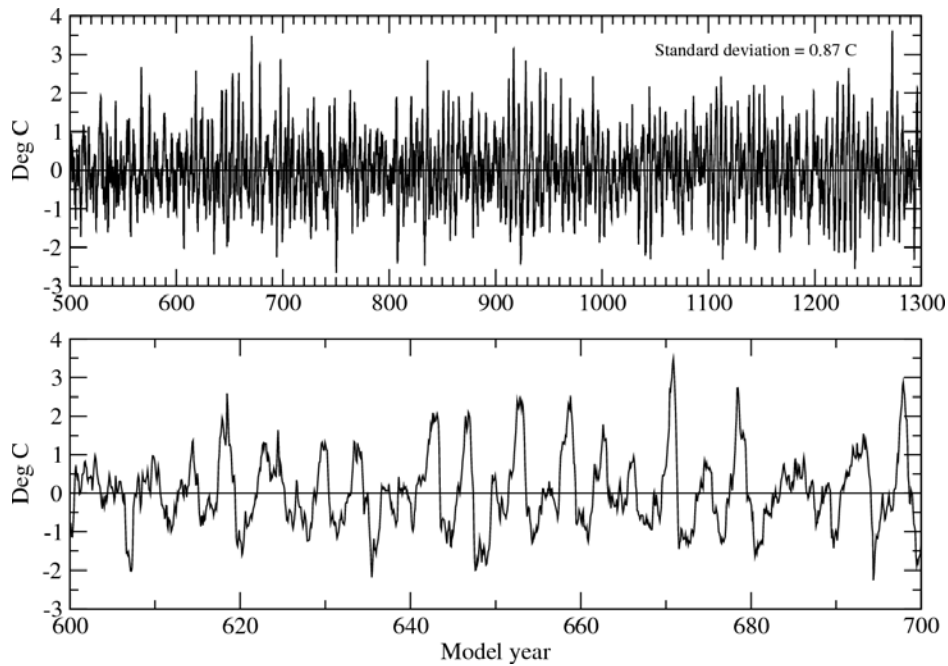


**Fig. 11a Modeled Nino3.4 temperature anomaly.**

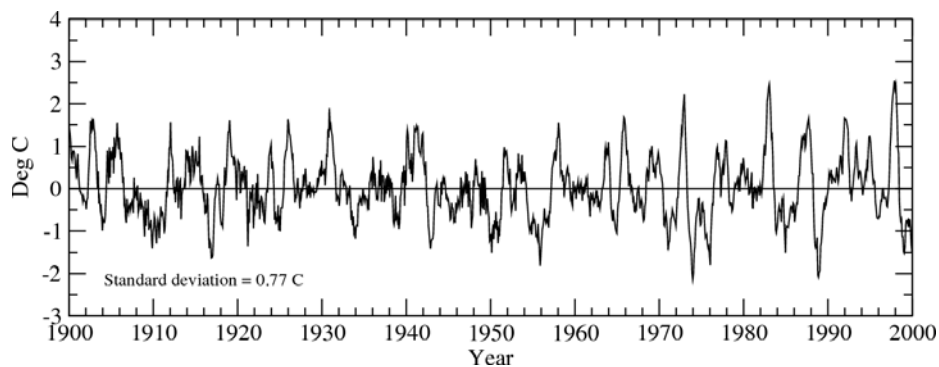


**Fig. 11b Observed Nino3.4 temperature anomaly.**

The modeled Nino3.4 data (Fig. 11a) has a small linear trend (upward) over the period. The trend amounts to 0.000206 degrees per model year (0.165 degrees over the 800 year period) and is in accord with the increase in global mean temperature seen in Fig. 9. The modeled SST anomaly in the Nino3.4 region ranges between about  $-2.5^{\circ}\text{C}$  to  $+3.5^{\circ}\text{C}$ . There is considerable variability in the anomaly over the entire period shown. The response over model years 600-700 is shown in the lower panel of Fig. 11a and highlights the considerable variability on a year by year basis (the data is plotted as monthly values). However, as the time series analysis indicates, there is a strong preference for a peak in the spectrum at about 4.9 years. The observed Nino3.4 temperature anomaly from 1900 to 2000 is shown in Fig. 11b. The modeled variability compares well to the observed variability. The standard deviation is  $0.77^{\circ}\text{C}$  in the observed time series, while the modeled standard deviation is a little larger at  $0.87^{\circ}\text{C}$ .

The spectrum of the Nino3.4 variability fluctuates considerably from epoch to epoch during the course of the Mk3.0 and Mk3.5 simulations. A comparison of the range of Nino3.4 spectra (for 50 year periods) for the Mk3.0 and Mk3.5 models is given in Fig. 12. For the Mk3.5 model, the number of 50 year periods was 12 (years 101 to 700), while for Mk3.0 the number of 50 year

periods was 9. Also shown is the observed spectrum in which there is a single period of 54 years taken from HadISST1 , years 1949-2002 ( <http://badc.nerc.ac.uk/data/hadisst> ).

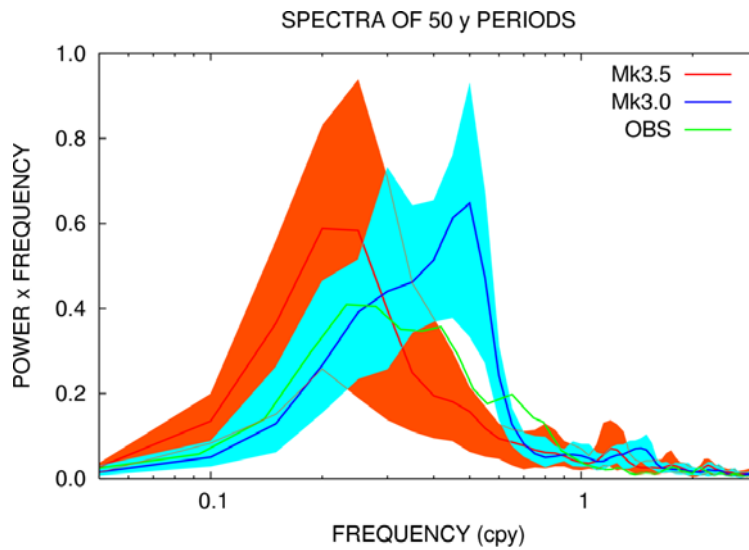


**Fig. 12 Nino3.4 temperature anomaly spectra (cpy = cycles per year: period in years given by 1/cpy).**

The observed Nino3.4 spectrum has two prominent peaks at about 4.4 years and 2.3 years. The Mk3.0 model had a strong preference for a peak at 2 years. On the other hand, the Mk3.5 model has a preference for a peak at about 4.9 years (a little longer than the observations) but lacks evidence of the peak at the shorter time scale (2.3 years) seen in the observations. Thus overall the Mk3.5 coupled model has a somewhat better correspondence to the observed Nino3.4 spectrum than the Mk3.0 model. However, the strength of the Nino3.4 signal is overestimated in both models, although less so in Mk3.5.

The composite of months with Nino3.4 values in excess of 1.5 times the standard deviation in the observations ( $1.5 * 0.77C$ ) for the period 1900 to 1999 is shown in Fig. 13. This shows the classic EL-Nino signal with a clearly defined positive maximum in the eastern tropical Pacific, with a “horseshoe” pattern of negative values to the north, west, and south.

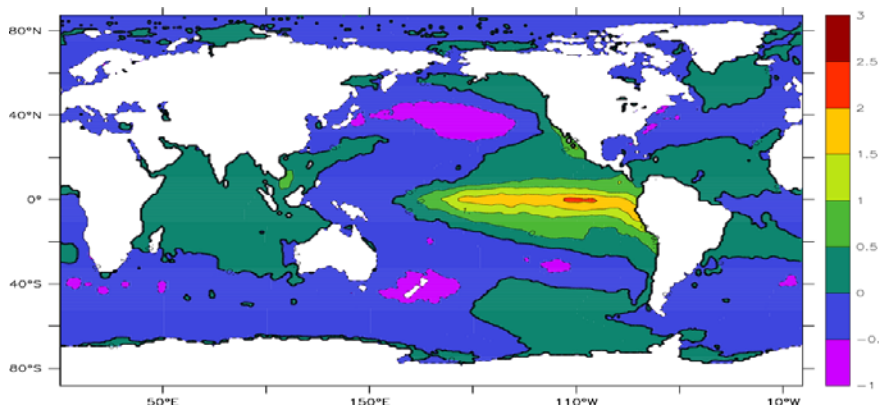


**Fig. 13 Composite of observed El-Nino events for years 1900-1999.**

A composite for the Mk3.5 coupled model run (years 600-699) of months with Nino3.4 values in excess of 1.5 times the *observed* standard deviation ( $1.5 * 0.77C$ ) is shown in Fig. 14. (The observed standard deviation of  $0.77C$  rather than the modeled standard deviation of  $0.87C$  was

used here so as to make the comparison of composites more compatible). The modeled El-Nino events have a similar pattern to the observed, but the location of the positive maximum is too far to the west. The observed maximum location is at about 110W, whereas the modeled maximum location is 180E. The El-Nino events in the model extend too far to the west, and the maximum value in the composites is too large at 2.6C compared to the observations at 2.1C.

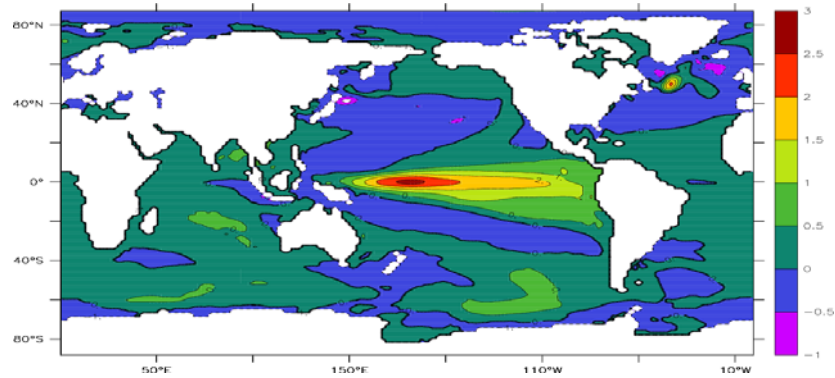


**Fig. 14** Composite of modeled El-Nino events for years 600-699.

### 8.4 Modeled SST compared to observations

During spin-up, the OGCM is constrained by the relaxation condition at the surface (relaxation to Levitus based observations). Upon coupling, the ocean surface responds to the heat flux supplied by the AGCM and also to associated feedbacks that were not present during spin-up. During the coupled model run, some differences between the modeled SST and the observed climatology are thus to be expected. The observed annual mean SST is displayed in upper panel of Fig. 15 and the annual mean (years 451-500) in Mk3.5 is displayed in the lower panel.

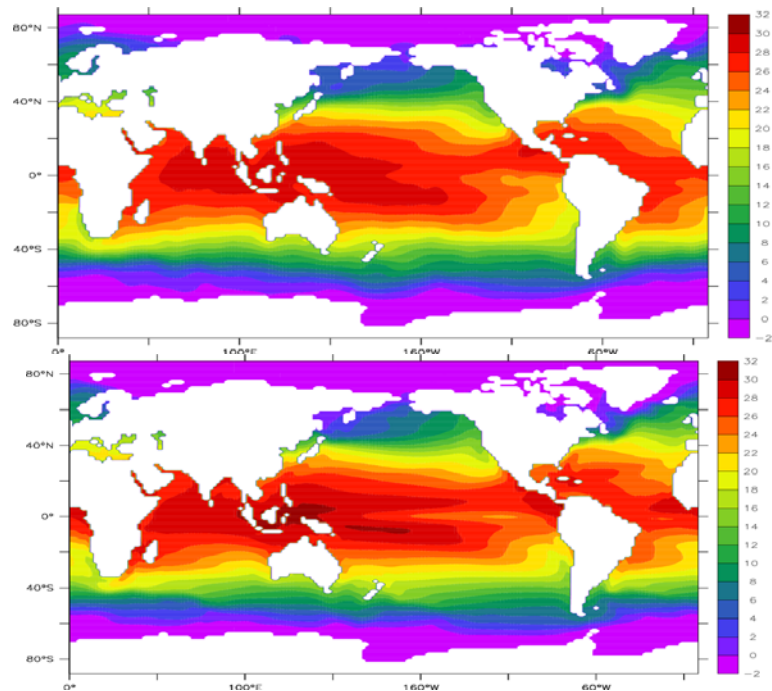


**Fig. 15** Annual mean SST: Observations (upper) and Mk3.5 (lower).

There is a reasonable degree of correspondence for much of the globe. However, there are areas of discrepancy that merit attention, such as in the tropical Pacific. These discrepancies are best illustrated by the use of difference maps. The global distribution of the difference between the coupled model SST and the observed SST is displayed in Figs 16a and 16b. In the first part (16a), the model averaging period comprises years 451-500, while in the second part (16b), the averaging period comprises years 1251-1300.

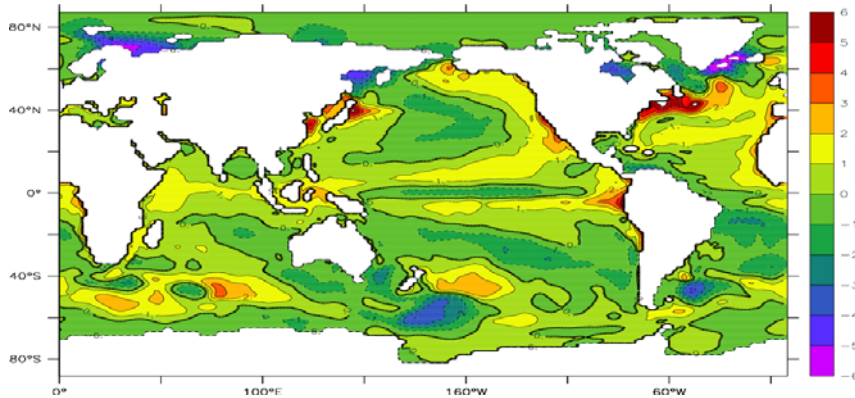


**Fig. 16a** Annual mean SST difference (°C): Coupled (451-500) minus Observations.

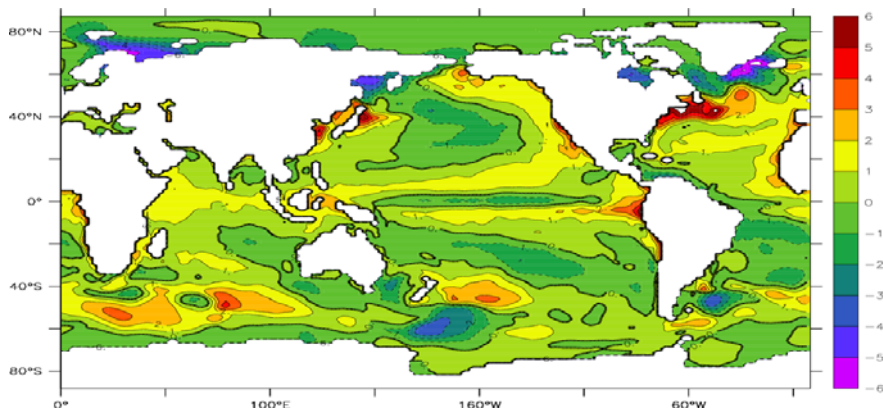


**Fig. 16b** As Fig. 16a, except Coupled (years 1251-1300) minus Observations.

These two figures (16a and 16b) are remarkably similar for much of the world ocean. This implies that the model has reached a fairly stable distribution of SST by year 500. With regard to the model SST compared to the observed SST, there are some clear model biases. The two figures show that there is some evidence of an over representation of the “cold-tongue” in the central Pacific (over 1°C). This cold-tongue problem is common to many coupled models (Mechoso et al. 1995; Meehl et al. 2001). However, the magnitude of the cold tongue error has been reduced relative to the Mk3.0 coupled model. This reduction has been brought about in part by the change to the surface drag formulation which now accounts for the velocity of the ocean currents relative to the atmospheric surface velocity. See subsection 4.1.4 for more details.

Another problem area for moderate resolution global coupled models is the positioning of the Gulf Stream and the Kuroshio Current. The North Pacific shows a sizable area which is colder than the observations by more than 1°C in the central part. This is a moderate improvement over

Mk3.0 which had errors of over  $2^{\circ}\text{C}$ . The Gulf Stream also shows some significant errors. The area to the south-east of Greenland is too cold, as is a region to the north of Finland. However, the sea-ice extent in the Arctic region is still reasonable (see later discussion). In the Southern Ocean, the region around Kerguelen shows a cool area to the northwest and a warm area to the southeast, which extends into the Antarctic Circumpolar Current down towards Antarctica. (A similar behaviour was also present in the Mk3.0 model in the vicinity of Kerguelen.) There are also prominent errors to the east of New Zealand, and east of South America. However, the southern extent of these SST errors does not appear to have a major impact on the Antarctic sea-ice (see later description in subsection 9.6).

## 8.5 Global mean SSS

The change in the global mean SSS over the 1300 year run is shown next (Fig. 17). Also shown are the relative changes in the NH and SH.

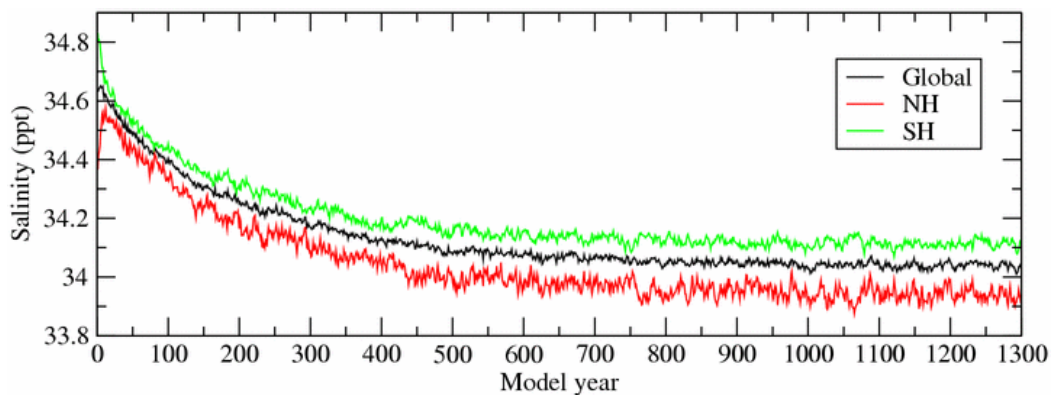


**Fig. 17 Global and hemispheric mean SSS.**

The response of the Mk3.5 model with regard to salinity changes upon coupling is inferior to that of the Mk3.0 model (see Mk3.0 Technical Report, Gordon et al., 2002). After coupling (year 0), the Mk3.5 couple model SSS undergoes an immediate change in both hemispheres with a decrease in mean salinity in the SH and an increase in the NH. There is then a gradual decrease in the SSS with most of the decrease being achieved in the first 500 year period. The change in mean salinity for the first 500 year period is  $-0.55$ , with a further decrease of about  $0.05$  to year 1300. This decrease in mean surface salinity is offset by an increase in salinity in the deep oceans. (The freshwater flux at the surface is practically zero over the period, and the global-vertical average of ocean salinity for the period is thus maintained.)

## 8.6 Modeled SSS compared to observations

The global distribution of the annual mean SSS from observations and as simulated (years 451-500) are displayed in Fig. 18.

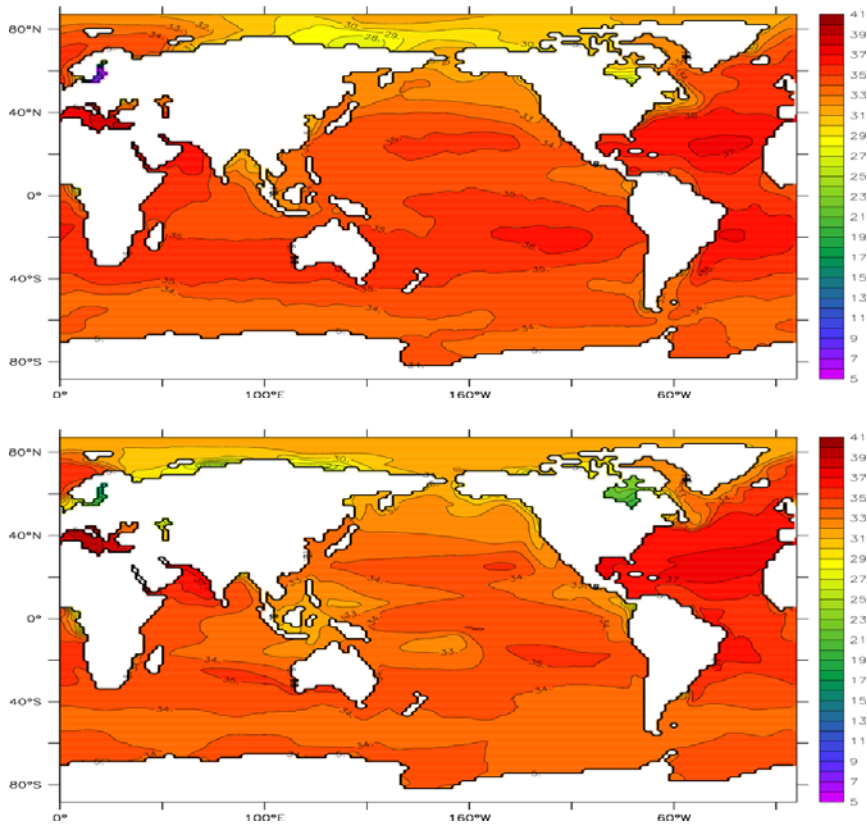


**Fig. 18 Annual mean SSS: Observations (upper) and Mk3.5 years 451-500 (lower).**

By model year 500, the main changes in the SSS have taken place and there are only relatively small changes from then to year 1300. The lower panel of Fig.18 shows that there has been freshening in the Pacific, especially in the tropics (the ITCZ region). The change in the SSS over the 1300 year period relative to the observed climatology is shown next as a difference map (Fig. 19).

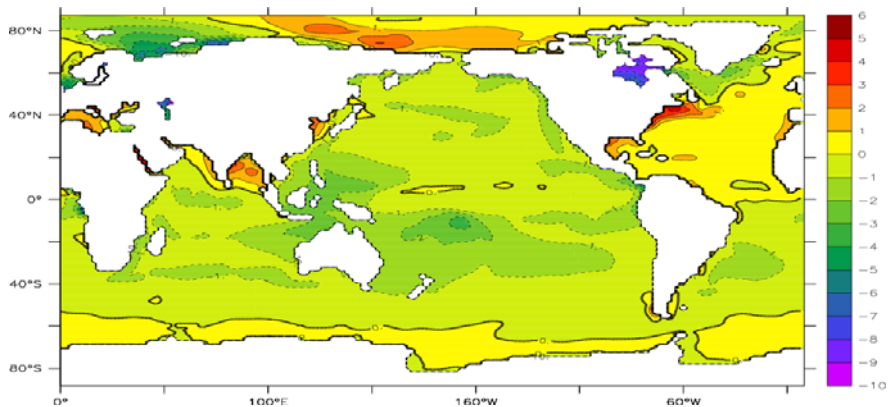


**Fig. 19 Annual mean SSS difference (ppt): Coupled (1251-1300) minus observations.**

The coupled model has become generally fresher at the surface. This occurs for large parts of the world. The central Pacific in particular shows an extensive area of freshening.

This area of surface freshening can be mainly attributed to increased precipitation. See subsections 9.8 (Surface Water Flux) and 9.9 (Rainfall) below for more details. The North Atlantic is one region that shows evidence of increased surface salinity.

The Hudson Bay has become fresher. This region does not have any imposed mixing (across land) to the North Sea. Thus a small amount of across-land mixing for salinity would appear to be required for the Hudson Bay (The passage to Hudson Bay in terms of the model grid resolution does not have a velocity vector present at one point in the passage). This type of across land mixing is already in use in the model for connecting the other (inland) seas to the world oceans (see subsection 5.1.6 in the model description).

Some of the changes in SSS can be related to changes in river outflow rates. For example, there are changes of both signs in SSS in the Arctic Ocean. The area of freshening at about 30 to 90°E is in a region that has undergone some cooling (see Figs 16a,b) and has more extensive sea-ice. However, this particular area of freshening appears to be associated with increased river runoff in the coupled model compared to spin-up, as illustrated in Fig. 20.

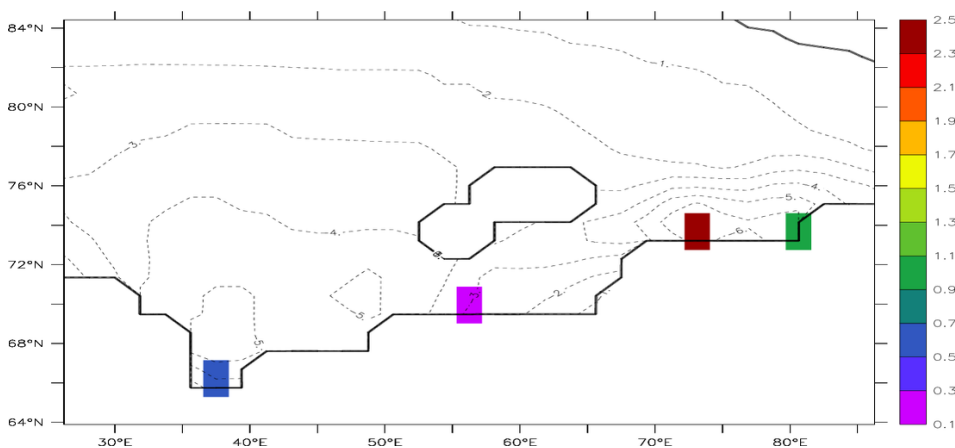


**Fig. 20** Change in Arctic Ocean river outflow rates ( $1000\text{m}^3 / \text{sec}$  shown by coloured boxes), and change in SSS (ppt shown by contours) by years 451-500.

The four major river outflow points (in modelling terms) are shown in the diagram. The freshening in this part of the Arctic Ocean (shown by negative contour values) has a clear correspondence to the increase in river outflow rates from various rivers in northern Russia. The largest increase in outflow (about  $2400 \text{ m}^3 / \text{sec}$ ) into the Kara Sea comes mainly from the Ob' river system (as represented by the river routing scheme in the model). This represents an increase of over 10% compared to AGCM spin-up.

## 8.7 Sea-ice volume

The sea-ice model in the CSIRO climate model is developed as a component part of the AGCM. The sea-ice is a key indicator of the performance of a climate model, and will clearly be sensitive to any discrepancies in temperature upon coupling. In Fig. 9 the coupled model in the NH showed some overall warming (about  $+0.6^\circ\text{C}$ ) over the first 300 years, while the SH showed some cooling (about  $-0.3^\circ\text{C}$ ). There was thus some change in the sea-ice cover and total

ice volume, especially in the NH. The sea ice volume for the Arctic and Antarctic are shown in Fig. 21.

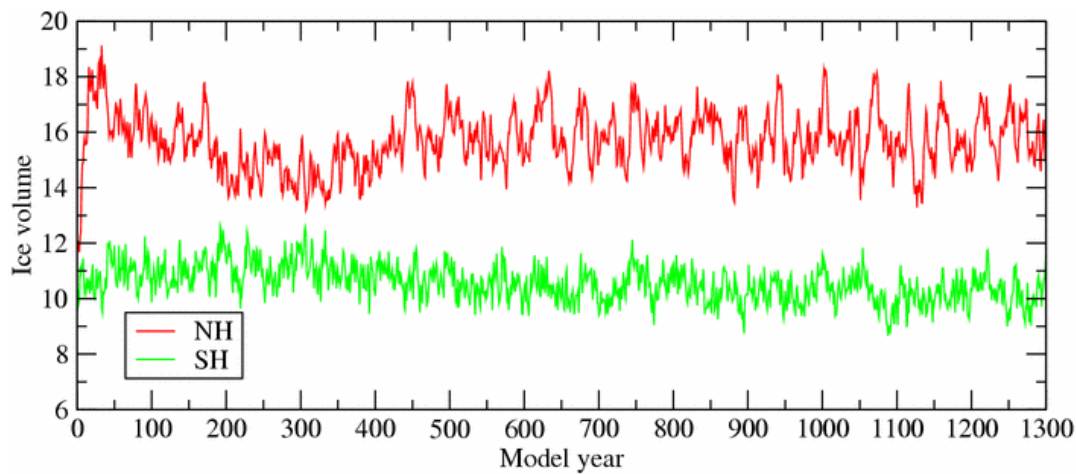


**Fig. 21** The coupled model NH and SH annual mean ice volume ( $10^3 \text{ km}^3$ ).

The SH ice volume (and cover) was not changed under coupled conditions relative to that in the AGCM spin-up. On the other hand, in the NH in the first 50 years there was a rapid increase from about  $12 (10^3 \text{ km}^3)$  at the end of the AGCM spin-up to  $18 (10^3 \text{ km}^3)$ . This was followed by a reduction to  $14 (10^3 \text{ km}^3)$  over 250 years, and then a slow increase to about  $16 (10^3 \text{ km}^3)$ . This contrast with the Mk3.0 model run which had an initial annual mean NH ice volume of  $18 (10^3 \text{ km}^3)$  followed by a very rapid increase to about  $40 (10^3 \text{ km}^3)$  after 15 years. The sea-ice cover and thickness (see below for the latter) is thus very well maintained in the Mk3.5 model over the 1300 year coupled run after an initial settling down period of 200 years.

As shown next, the horizontal extent of the sea-ice coverage and seasonal cycle did not alter a great deal between uncoupled and coupled conditions in either hemisphere. The SH ice cover during the AGCM control run and in the Mk3.5 coupled run is shown in Fig. 22, while Fig. 23 shows the NH responses. The September and February ice extent is shown for the SH, and the April and September for the NH which represent the seasons of maximum and minimum extent. The AGCM ice cover data is from a 10 year control run, while the coupled data is from model years 1281 to 1300.

In the SH the seasonal ice extent and thickness patterns are very similar in both simulations with maximum ice thickness on the western coasts of the Weddell and Ross Seas. Both model climatologies are realistic compared to observations.

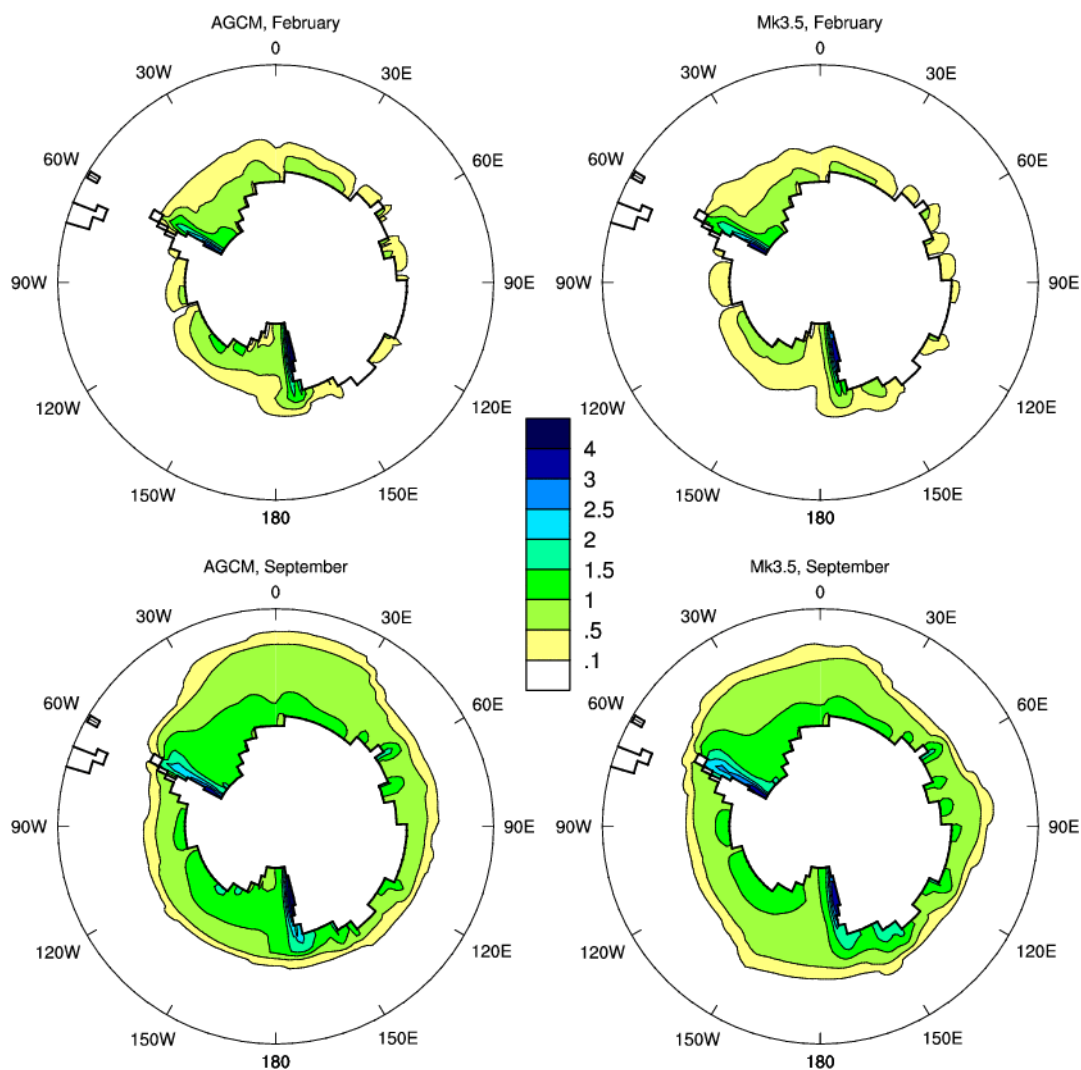


**Fig. 22** The SH ice thickness (m) for the AGCM spin-up and the Mk3.5 coupled run.

In the NH the ice thickness has increased only a little in the coupled model. The seasonal ice extent is similar in the North Pacific sector but is more extensive in the Greenland and Barents seas in the winter season. This increased ice cover is consistent with the cooling shown in both these regions in Figs 16a,b. The observed pattern of ice thickness (not shown) is derived from submarine data and indicates a maximum to the north of Greenland and along the Canadian Archipelago. Neither the ice-atmosphere model spin up nor the coupled model match this distribution satisfactorily. As noted in the technical report for the Mk3.0 model (Gordon et al., 2002), a possible cause for this may be that the atmospheric model winter wind stress climatology is not realistic. A realistic maximum NH ice volume is of the order of  $30 \times 10^3 \text{ km}^3$ , and so in the Mk3.5 coupled model the NH ice volume is somewhat too small, but rather better than the corresponding AGCM control run. Overall, the sea-ice responses in the coupled run have been remarkably stable over the 1300 year period.

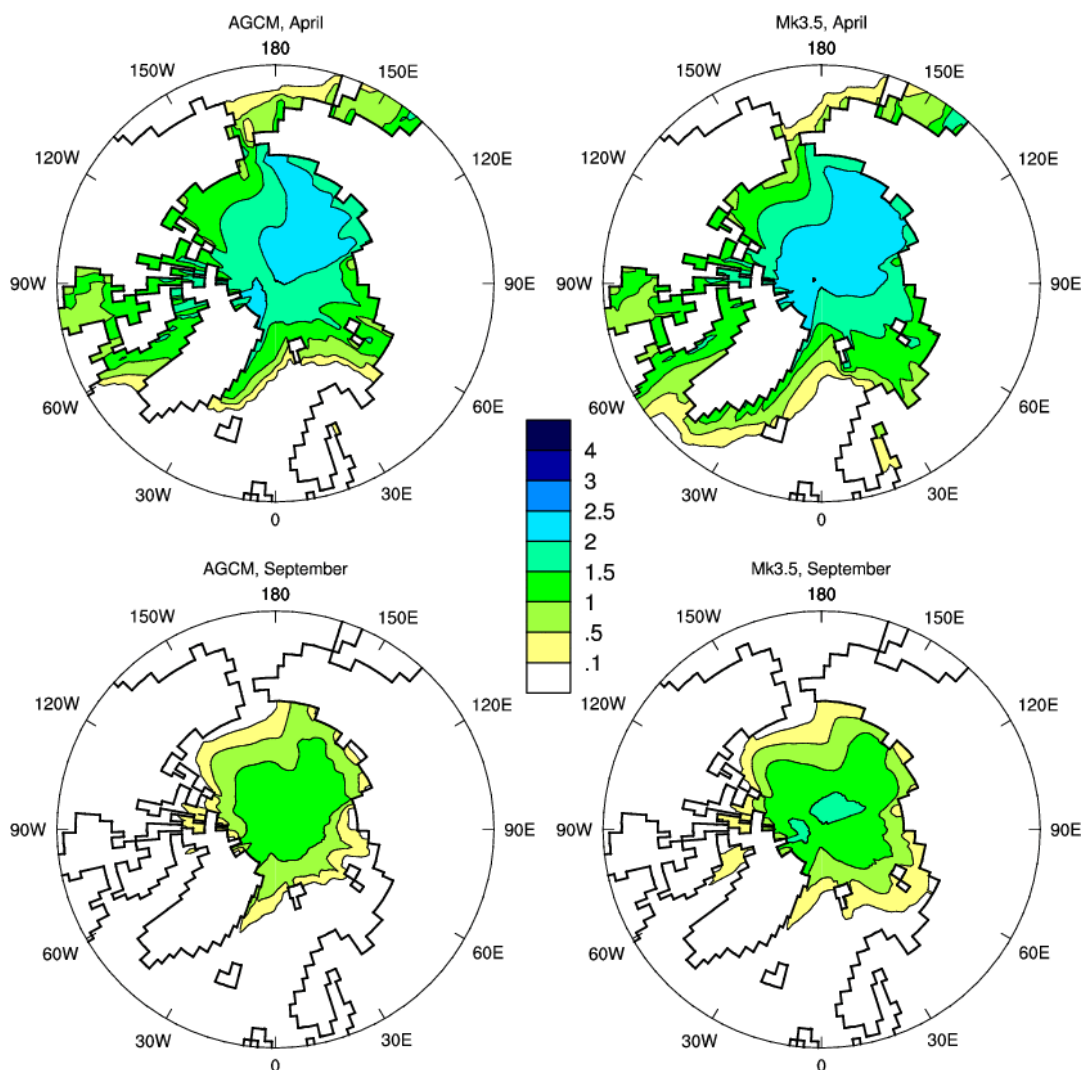
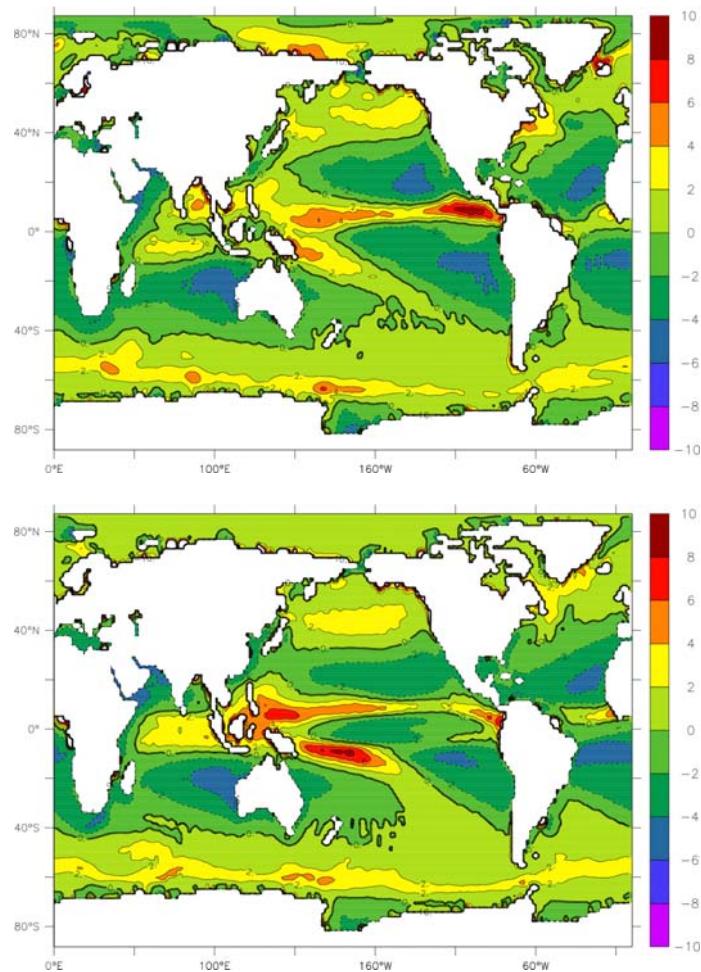


Fig. 23 The NH ice thickness (m) for the AGCM spin-up and the Mk3.5 coupled run.

## 8.8 Surface water flux

The change in salinity distribution at the surface following coupling is affected by changes in the surface fresh water flux between spin-up and coupling. It will also be affected by changes in other processes such as ocean overturning rates. The freshwater flux in the coupled model is a combination of three components: precipitation minus evaporation (P-E), river runoff, and water fluxes due to sea-ice freezing/melting processes. In the ocean model spin up, there is a freshwater flux implied by the relaxation at the surface to the observed (Levitus), seasonally varying, salinity distribution. (See section 7 for details about Mk3.5 spin-up conditions which used a combination of relaxation and AGCM surface fluxes).



**Fig. 24 Freshwater flux (in units of mm/day rainfall equivalent).** For spin-up (top) and coupled (below)

The annual mean freshwater flux for spin-up and coupled conditions (years 1251-1300) are shown in Fig. 24. In this figure, the freshwater flux is only displayed between  $\pm 10$  mms/day. (There are considerably larger positive fluxes for the freshwater flux at river outflow grid points (e.g., the Amazon).) The spin-up (implied) freshwater flux and the coupled freshwater flux have broad scale similarities for much of the globe, but there are regions which have significant differences. The tropical Pacific in the coupled model shows the largest differences in distribution. There is a much larger flux in the ITCZ to the north-east of Australia. This corresponds to the freshening in that region seen in Fig. 19. The Baltic Sea, which became more saline (increasing from about 8 ppt to 18 ppt at the surface), has a reduced average freshwater flux in the coupled run (4.6 mm/day) relative to spin-up (8.6 mm/day). In the Hudson Bay, which became less saline, the freshwater flux was larger in the coupled run (2.2 mm/day) than in the spin-up (0.4 mm/day). The change in the salinity is partly caused by the freshwater flux under coupled conditions (P-E and river runoff) not matching the freshwater flux implied by partial relaxation conditions under spin-up.

## 8.9 Rainfall

Some of the coupled model responses at the surface discussed above, particularly changes in sea surface salinity, may be linked to changes in the precipitation (rainfall and snowfall) patterns in the model. The Mk3.5 modeled precipitation is shown in Fig. 25 for the seasons of Dec-Feb, and Jul-Aug. For comparison, the observed precipitation (Xie and Arkin 1997) is also shown in Fig. 25. (The gridded data for this observational data set is available by anonymous ftp from <ftp.ncep.noaa.gov> and is in the directory /pub/precip/cmap/ ).

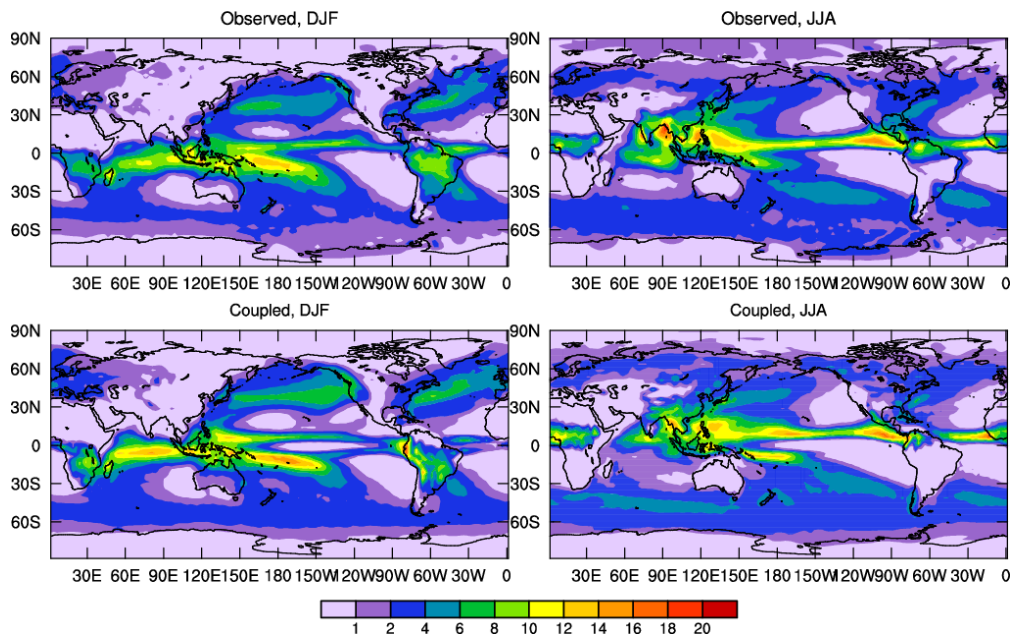


**Fig. 25 Rainfall (mm/day): Observations (Xie and Arkin, 1997) and coupled model (years 1281-1300); December-February on left and June-August on right.**

The Mk3.5 coupled model reproduces the observed rainfall pattern with a considerable degree of realism in both seasons (DJF and JJA). However, there are some important differences. In DJF, in the tropical Pacific the Mk3.5 coupled model still has a double, rather than a single ITCZ. This appears to be a common problem with coupled models which have a too pronounced cold tongue in the tropical SSTs. The colder water along the equator, with warmer water to either side causes the tropical convection centres to be moved over these warmer waters (see below). Over South America, there is a tendency for the rainfall to be too strongly centred over the higher topography regions. There also appears to be too much rainfall in the India Ocean, especially in DJF. In JJA, the Indian monsoon is not strong enough, although in the uncoupled AGCM, the Indian monsoon is much closer to the observed pattern (not shown). Thus the coupled model JJA SST pattern is having some adverse effect on the monsoon.

The difference between annual average rainfall from the coupled versus the uncoupled simulations is shown in Fig. 26. This shows that the largest change in precipitation occurs in the tropical regions. There is a reduction in rainfall along the equator in the Pacific which is associated with the cold tongue (see Fig. 16a,b) being up to 2°C too cold across the Pacific. The positive rainfall anomaly on both sides of the cold tongue coincides with the coupled model SSTs being warmer than observations, and also reflects the shift in the position of the maximum

rainfall towards the east. The greatest reduction in rainfall occurs in the eastern Pacific next to Central America. (The change in the zonally averaged annual mean rainfall between the stand alone Mk3.5 AGCM and the coupled model for ocean areas is shown later in Fig.39.)

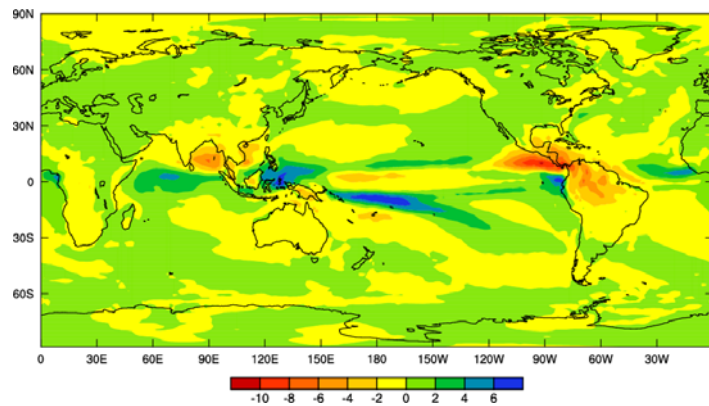


**Fig. 26 Annual precipitation (mm/day): Mk3.5 coupled model – Mk3.5 AGCM.**

The differences in rainfall patterns over land areas affects the river outflow rates into the world oceans. The Mk3.5 model uses an improved river routing scheme, and details are given in an Appendix (section 12). The following table (2) lists the main rivers and the outflow rates for the Mk3.5 AGCM (uncoupled) and the coupled Mk3.5 model. The observations are taken from Dumenil et al. (1993). There was a significant reduction in rainfall over the Amazon basin in the coupled model. This is reflected in the coupled annual average Amazon outflow rate being reduced to 41% of the (uncoupled) AGCM value. However, the Amazon outflow was too strong in uncoupled mode, while the coupled value is now too weak.

**Table 2. River outflows (1000m<sup>3</sup> sec<sup>-1</sup>)**

<b>River outflow</b>	<b>Observed</b>	<b>AGCM</b>	<b>Coupled</b>
Amazon	155	242	100
Congo	40	101	71
Ganges+Bramaputra	34	40	27
Orinoco	31	24	6
Yangtze	29	13	12
Yenisey	18	21	23
Lena	17	11	12
Parana	16	41*	29*
Baltic	15	10	11
St. Lawrence	8	12	12

\* Model grid point includes R. Uruguay outflow

## 8.10 Vertical mean ocean salinity

The mean change in salinity in the vertical is shown in Fig. 27. Here the salinity is plotted relative to model level in the vertical (there are 31 levels). (The depths of the ocean model levels are shown in Table 1 in section 5). The ocean has become more saline for the deep ocean (level 20 and below, i.e., at depths greater than about 1km). The coupled model is thus not mixing enough freshwater into the deep ocean. This is possibly related to insufficient overturning around Antarctica (see later) in the coupled model run. It may also be brought about by inadequacies in the vertical mixing schemes used in the model.

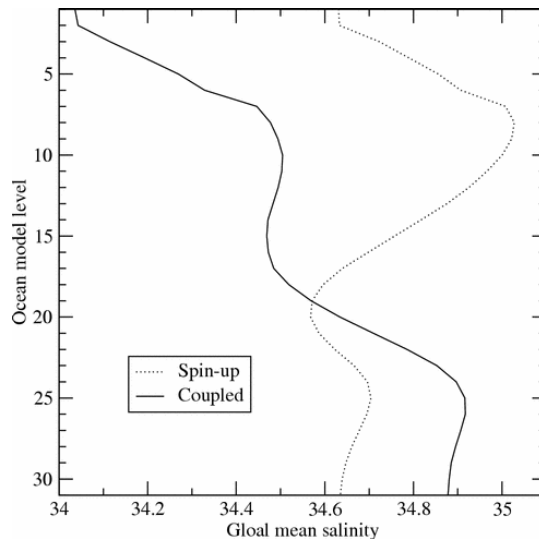


**Fig. 27 Global mean salinity per model level (50 year average): Ocean model spin-up and at end of coupled model run.**

The zonally averaged change in salinity (relative to the OGCM spin up) is shown in Fig. 28. This is the change by the end of the 1300 year run. This reflects the change shown in the previous figure (27). This particular figure has the depth of the ocean as the vertical axis

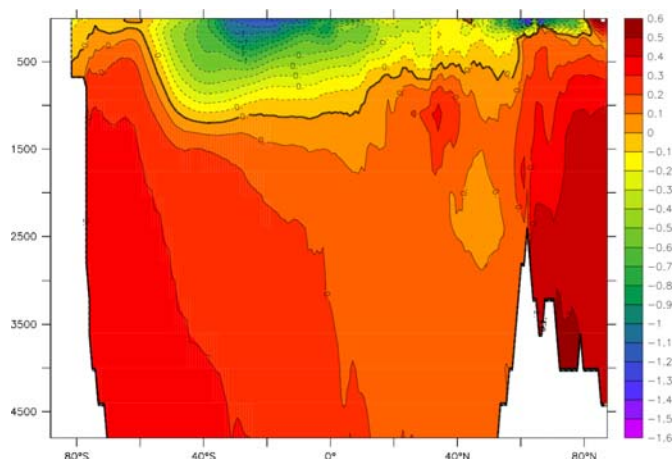


**Fig. 28 Change in zonally averaged salinity: End of coupled run minus ocean model spin-up (50 year averages).**

The increase in salinity north of 60°N mainly reflects an increase in salinity in the Arctic basin. The increase in salinity is up to 0.4 ppt below 1000m. It is least prominent in the Pacific Ocean. There appears to be insufficient overturning of cold, relatively less saline water in the Southern Ocean leading to a general increase in salinity in the deep oceans, while the near surface water (above 1000 m depth) has become fresher, especially between the equator and 40°S. This particular long term response of the coupled model (freshening at the surface and an increase of salinity with depth) may reflect inadequacies in the overturning and vertical/horizontal mixing in the current model.

## 8.11 Stream function and overturning rates

During the course of the coupled model run, the ocean is no longer under spin-up conditions (relaxation of surface temperature and salinity to observations together with AGCM surface fluxes). It is thus to be expected that there will be some change in the overall circulation of the ocean. This can be illustrated by means of the stream function and the overturning rates.

The depth-integrated stream function in the spin-up and in the coupled model runs for both Mk3.0 and Mk3.5 are shown in Fig. 29. The coupled model run data is taken from a 10-year average over years 110-120.

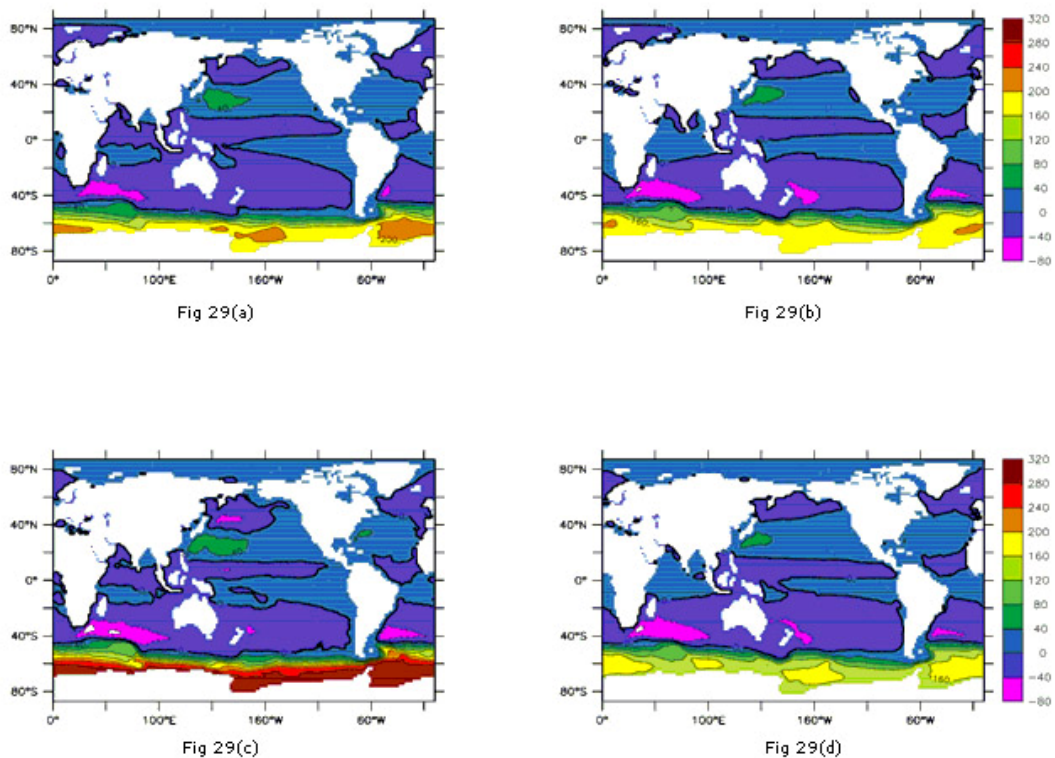


**Fig. 29** Ocean depth-integrated stream function ( $S_v$ ) for (a) Mk3.0 ocean spin-up; (b) Mk3.5 ocean spin-up; (c) Mk3.0 coupled, y111-120; (d) Mk3.5 coupled, y111-120..

Comparing the upper two panels (Mk3.0 and Mk3.5 OGCM spin-up), it is seen that Antarctic circumpolar stream function value is a little reduced in the Mk3.5 spin up relative to Mk3.0. In the Mk3.0 coupled run there was a significant increase in the circumpolar stream function by year 80, with some further strengthening for the next 200 years (to an annual average value of

about 310 Sv for the Drake Passage throughflow). In contrast, in the Mk3.5 coupled run, there was only a small reduction in strength by year 120, and during the rest of the 1300 year run the strength did not change appreciably. The annual average value of the Drake Passage throughflow was in the range 150 to 160 Sv, compared with the observed value of order 130 to 140 Sv, and thus the Mk3.5 coupled model performs much better than Mk3.0 with regard to the strength of the Antarctic Circumpolar Current.

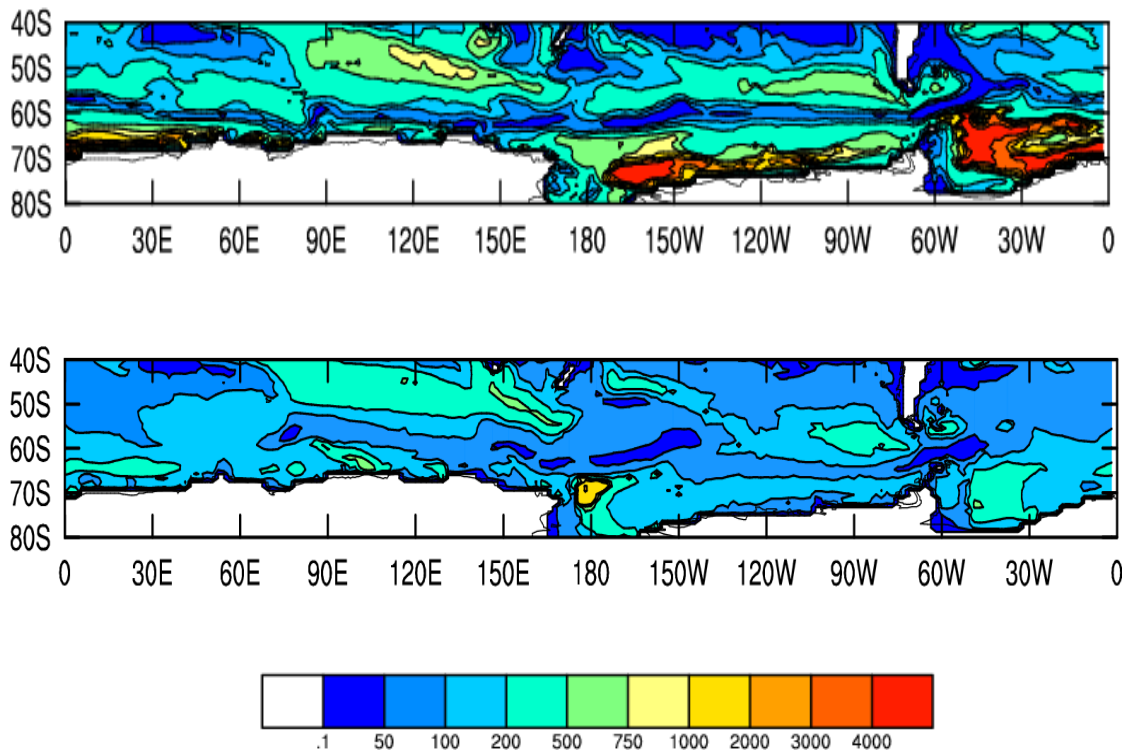


**Fig. 30 Mean mixed layer depths in the Southern Ocean for September calculated from Mk3.0 (upper panel) and Mk3.5 (lower panel) monthly density fields .The mixed layer depth was taken as the depth at which  $\sigma_\theta$  first exceeded its surface value by more than  $0.125 \text{ kg m}^{-3}$ .**

The reduction in the strength of the Antarctic Circumpolar Current in the Mk3.5 model is associated with other major changes in the circulation of the Southern Ocean. Figure 30 shows the late winter (September) mixed layer depth over the Southern Ocean in Mk3.0 and Mk3.5. Observed late winter mixed layers are mostly shallow (order 50-500 m depth) over most of the high latitude Southern Ocean (e.g., Monterey and Levitus 1997). In contrast, the Mk3.0 solution displays extensive very deep convective mixed layers over parts of this region. The Mk3.5 solution displays much shallower, more realistic, mixed layer depths. The realism of mixing in the Southern Ocean is likely to be important in the realistic simulation of oceanic heat uptake and regional surface warming rates under global warming.

The change in mean circulation in the oceans can also be illustrated through the mean meridional overturning. In Fig. 30, the annual mean overturning in the NH is shown for spin-up conditions (average over last 10 years) and at the end of the coupled period (average over years 1251-1300).

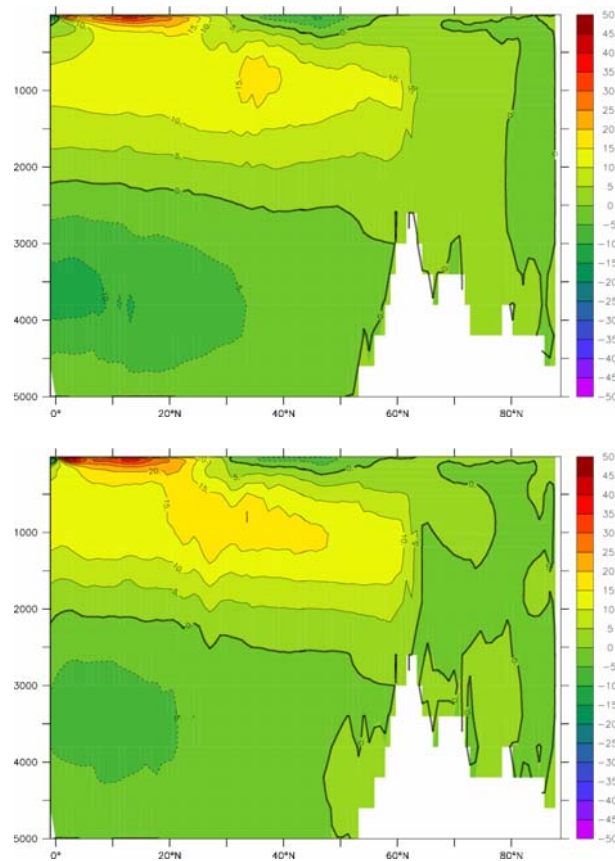


**Fig. 31 NH vertical-meridional streamfunction (Sverdrups): End of ocean spin-up (upper) and coupled model, years 1251-1300 (lower).**

It is seen that the North Atlantic cell of North Atlantic Deep Water (NADW) has achieved a more realistic amplitude (e.g., Sime et al., 2006) with sinking at  $55^{\circ}\text{N}$  increasing to 15Sv, though NADW still does not penetrate deep enough into the ocean in the North Atlantic basin.

The overturning in the Southern Hemisphere (end of spin-up and coupled model years 1251-1300) is shown in Fig. 31. The stream-function in the Mk3.5 coupled model at  $70^{\circ}\text{S}$  is much weaker than in the spin-up (about 5 Sv) and in the Mk3.0 coupled model (see Fig. 12 of Gordon et al. (2002)). The cause of this weakening in the overturning streamfunction is yet to be clearly determined. Factors may include changes in ocean model physical parameterizations between Mk3.0 and Mk3.5, and changes in the surface fluxes from ocean spin-up upon coupling in the Mk3.5. Oceanic parameterization changes include the use of Visbeck and Kraus-Turner parameterizations, extra horizontal mixing in specific locations (land-sea boundaries), and a horizontal mixing parameterization based on curl of surface stress (see subsections 5.1.1 to 5.1.8 above).

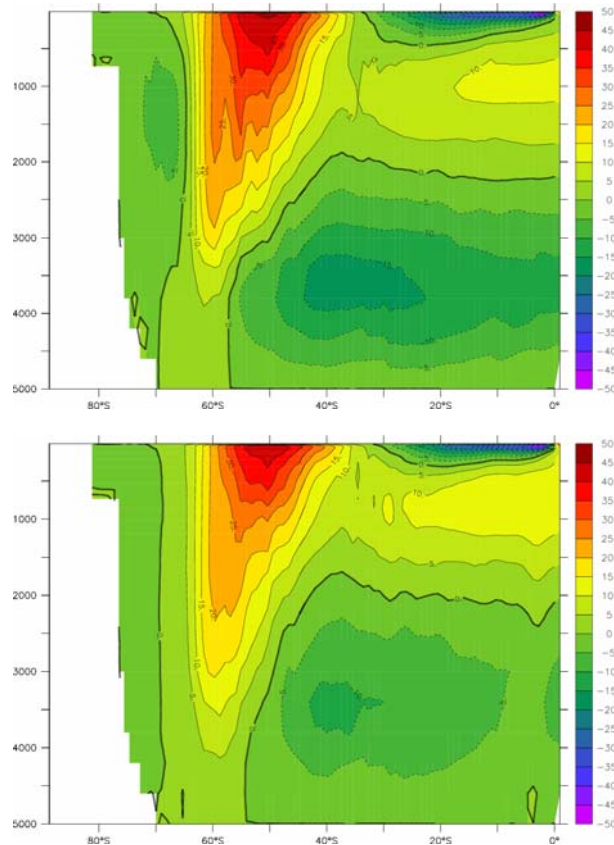


**Fig. 32 SH vertical-meridional streamfunction (Sverdrups): End of ocean spin-up (upper) and coupled model, years 1251-1300 (lower).**

In the following sections, we present an analysis of the impact of the physics changes between Mk3.0 and Mk3.5 and the transition to coupling on the oceanic surface freshwater and heat fluxes. The analysis is global, however we pay particular attention to the flux differences adjacent to Antarctica, to attempt to shed some light on the causes of the differences in the strength of Antarctic overturning. The overturning is governed by the surface waters becoming dense enough to cause sinking. The density at the surface is affected directly by the local heat flux and water flux. Due to the changed conditions upon coupling, it is to be expected that the surface heat flux and water flux will be modified by various feedback processes. Thus when assessing the possible causes of changes in model climatology after coupling takes place, the surface fluxes merit particular attention.<sup>3</sup>

## 8.12 Assessing changes in OGCM parameterizations

Some separate runs of the stand alone OGCM and the of the coupled model (results not included here) were undertaken in which the extra horizontal mixing parameterizations in Mk3.5 (as described in subsections 5.1.3, 5.1.4, and 5.1.5 above) were turned off. These particular parameterizations were for mixing applied in specified locations (5.1.3), mixing via the curl of the surface stress (5.1.4), and a Visbeck dependent upper ocean diffusion process

<sup>3</sup> A more complete analysis of the overturning forcing by surface fluxes would involve calculation of surface buoyancy fluxes and meridional overturning in density coordinates, but that is beyond the scope of the present report.

(5.1.5). It was found that the removal of these particular parameterizations did not have a significant effect on the zonal average surface heat fluxes in the near Antarctic region.

On the other hand, the use of the Visbeck and Kraus-Turner schemes (see subsections 5.1.1 and 5.1.2) in the Mk3.5 ocean model did have an impact on the general climatology of the ocean model (relative to Mk3.0) with some appreciable changes to the local and zonal averages surface heat and water flux requirements.

To clarify the difference in (implied) surface flux requirements during spin-up of the Mk3.5 OGCM relative to Mk3.0, the Mk3.5 OGCM underwent a spin-up with a similar set-up to that used in the Mk3.0 OGCM spin-up. The AGCM surface fluxes were set to zero (i.e. removed) and the relaxation damping times for T and S were both set at 6 days (to be compatible with the Mk3.0 OGCM spin-up). A comparison of the (implied) surface water and heat fluxes for the modified Mk3.5 OGCM spin-up (denoted by Mk3.5#) and the Mk3.0 spin-up is shown in Figs 32 and 33.

The surface water fluxes are similar at most latitudes, with the largest differences being in the high northern latitudes. In particular, the large negative water flux requirement (about -10 mms/day) in the Arctic in the Mk3.0 OGCM spin-up is not evident in the Mk3.5 OGCM spin-up. This indicates that the modifications to the OGCM physical parameterizations may have had a beneficial effect on the OGCM in the high latitudes of the northern hemisphere. There is little difference in the zonal average water flux requirements near Antarctica.

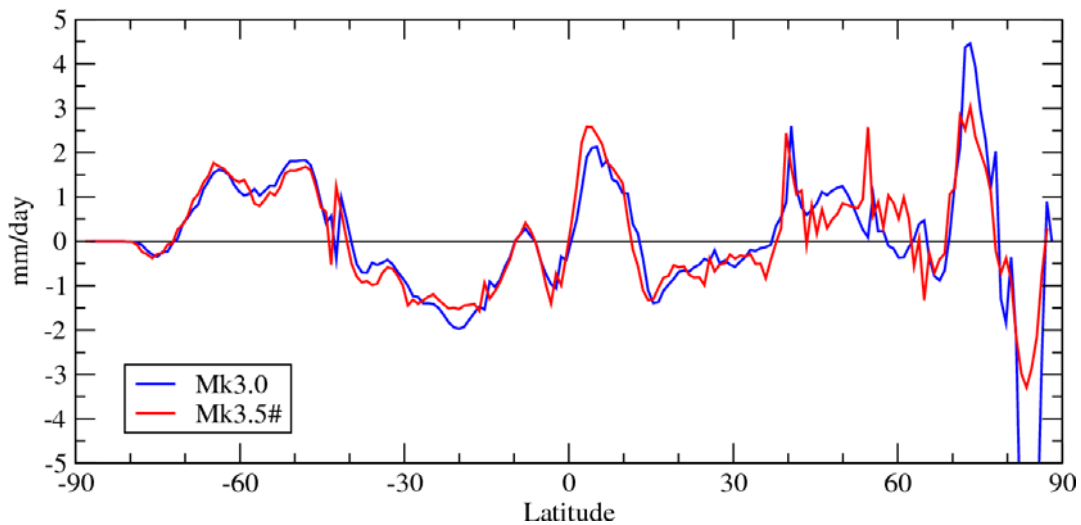


**Fig. 33** The zonal average surface water flux for Mk3.0 OGCM spin-up and Mk3.5# OGCM spin-up (# indicates no AGCM heat/salt fluxes). (Note: In Figs 32-40, the zonal average flux is calculated as the zonal integral of the flux divided by the zonal circumference at that latitude.)

The implied surface heat fluxes (Fig. 33) show some differences for the mid-latitudes in both hemispheres. Thus the use of the Visbeck and Kraus-Turner parameterizations are having some impact on the surface heat flux requirements. However, near Antarctica, the difference in zonal average heat flux is not very large (a few  $W/m^2$  more cooling is required in the Mk3.5# case). So, inspection of the solutions of the stand alone OGCMs may not necessarily reveal the disparity in Antarctic overturning that develops between the solutions of the Mk3.0 and Mk3.5 coupled models.

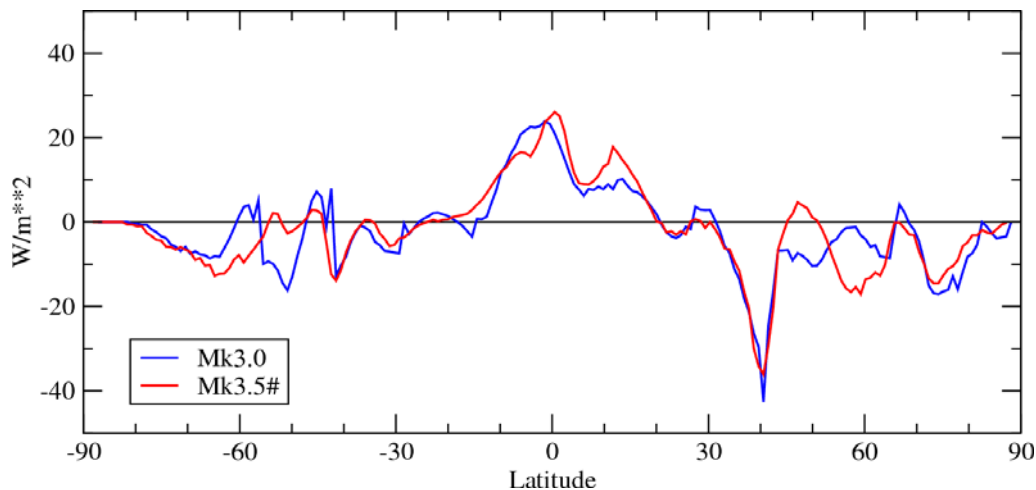


Fig. 34 As in Fig. 32 except for surface heat fluxes.

### 8.13 Surface fluxes before and after coupling

Next we consider the Mk3.5 surface heat and water fluxes implied (or generated) by the AGCM and OGCM components in two parts: The fluxes *before* coupling are denoted as F1 fluxes, while those generated *after* coupling are denoted as F2 fluxes. The F1 fluxes are those implied by the stand alone OGCM and those generated by the stand alone AGCM. The F2 fluxes are those generated by the coupled model when various model feedbacks come into play.

#### F1 - Stand alone surface fluxes:

The Mk3.5 OGCM before coupling is driven by relaxation conditions for temperature and salinity at the surface, together with AGCM surface fluxes. The relaxation time scale for temperature is 6 days and for salinity it is 200 days. The spin-up of the OGCM thus generates an implied surface flux of heat that is required to maintain the ocean model climatology close to that of Levitus SST because of the short prescribed relaxation timescale. Due to the longer prescribed relaxation timescale for surface salinity, the surface water flux does not necessarily keep the SSS distribution as close to Levitus.

On the other hand, the stand alone AGCM, driven by the prescribed annual cycle of SSTs, generates water and heat and fluxes at the atmosphere-ocean (or ice-ocean) interface by direct computation of the various components that make up the total flux.

A comparison is now made of the OGCM and AGCM surface fluxes generated during the spin-up of these models. Fig. 34 compares the (uncoupled) zonally averaged AGCM and OGCM surface water fluxes, while Fig. 35 compares the surface heat fluxes.

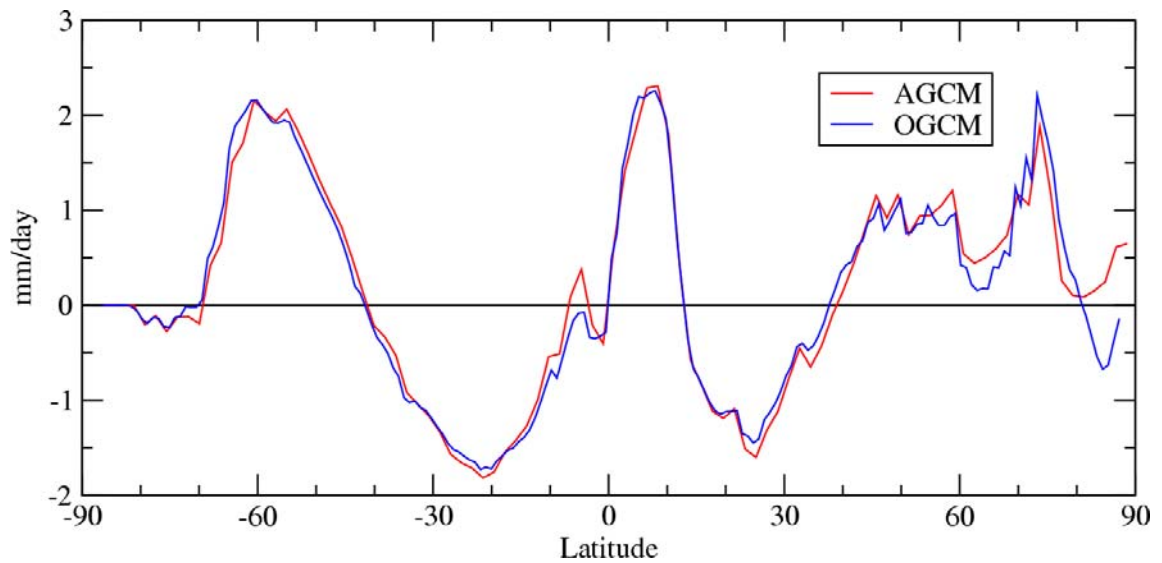


**Fig. 35 The surface water fluxes for stand-alone AGCM and OGCM.**

The AGCM and OGCM surface water fluxes in Fig. 34 are quite similar because the OGCM is being driven by AGCM fluxes, together with only a relatively weak relaxation component (200 days) for SSS.

The F1 surface heat fluxes shown in Fig. 35 do not have the same correspondence shown for the surface water fluxes, and this is due to the stronger relaxation component (6 days) for SST in the OGCM spin-up. However, the zonally averaged AGCM and OGCM surface heat fluxes are not dissimilar for most latitudes.

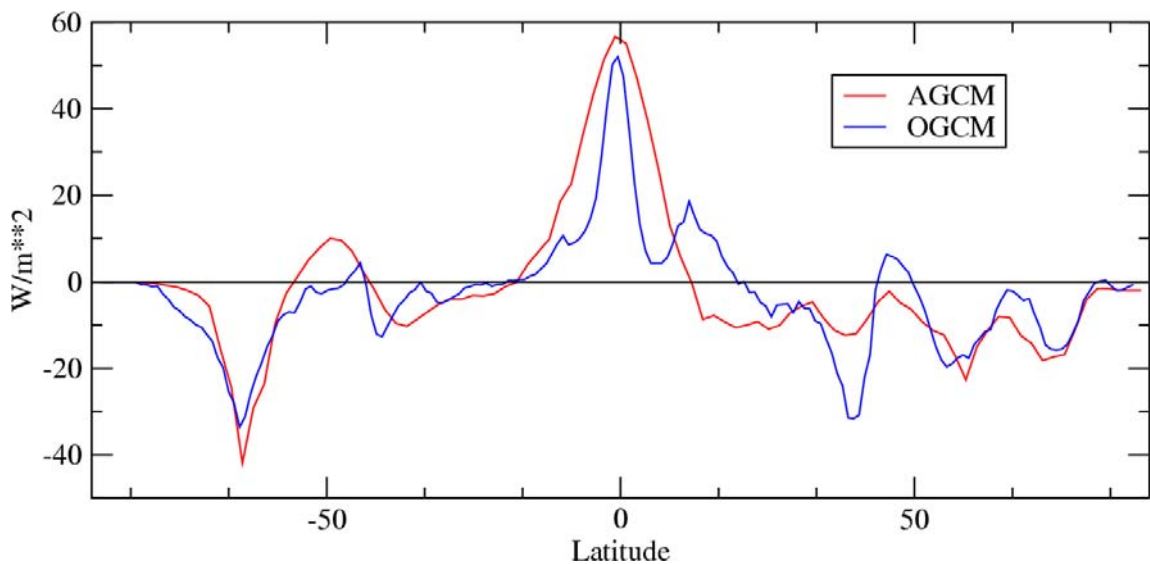


**Fig. 36 The surface heat fluxes for stand-alone AGCM and OGCM.**

The Mk3.5 OGCM spin-up, when forced at the surface by the combination of AGCM fluxes together with relaxation to Levitus, produced some overturning in the Antarctic region (see top panel of Fig. 31 above), and also maintained a vertical salinity distribution that was in

reasonable accord with the Levitus vertical profile. When changing to coupled mode (see next), the AGCM surface heat flux, having a zonally averaged profile somewhat different to the OGCM zonally averaged profile, would be expected to cause some change to model climatology following coupling.

## F2 – Surface fluxes after coupling:

The feedbacks between the coupled model components lead to some adjustment of the surface fluxes relative to those in the uncoupled AGCM. The coupled model surface water and heat fluxes are shown in Figs 36 and 37 respectively. The coupled model fluxes are taken from an average over years 21-40 of the Mk3.5 run. (A comparison of fluxes for years 21-40 and years 81-100 showed very similar zonally averaged profiles). Also plotted are the stand alone AGCM and OGCM fluxes for comparison.

The zonal surface water flux in the coupled model is very similar to that in the spin-up, with the exception being the tropics, which has been affected by changes in large scale rainfall patterns (see later discussion of rainfall changes). The water flux in the Antarctic region has become a little less negative. This aspect will be discussed in more detail below.

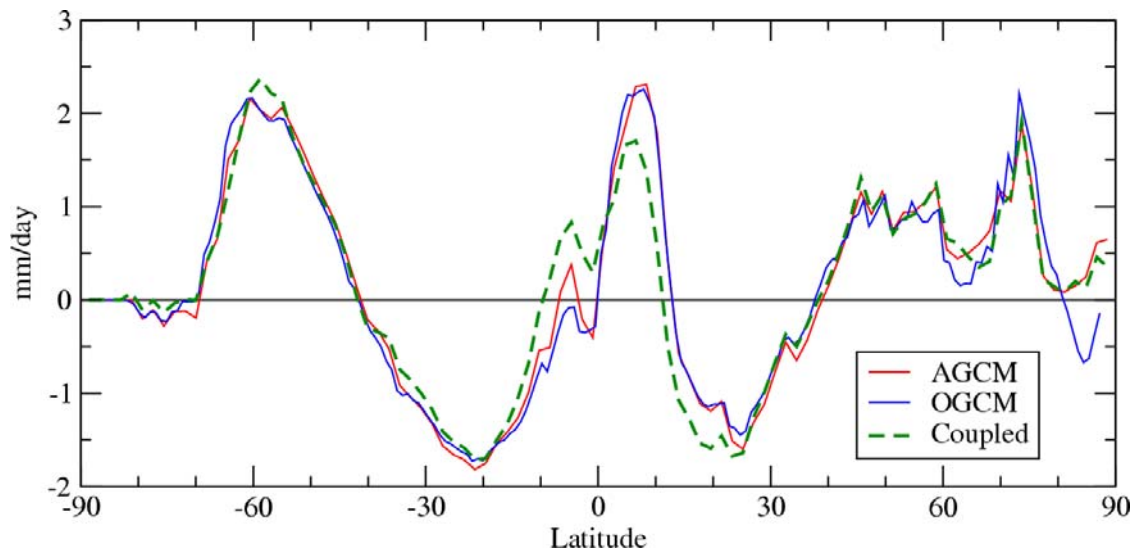


**Fig. 37 The surface water flux for the Mk3.5 coupled model, together with stand-alone AGCM and OGCM fluxes.**

The zonal surface heat flux in the coupled model (Fig. 37) turns out to be quite similar to that being generated by the stand alone OGCM, and less similar to the stand alone AGCM. Thus the feedbacks in the coupled model have apparently resulted in a heat flux that is more compatible with stand alone OGCM requirements for maintaining a suitable SST distribution. This is part of the reason for the small amount of SST drift in the Mk3.5 model run over 1300 years. In the Antarctic region (60°S to 80°S), the coupled model heat flux is a little different to that in the stand alone OGCM with the main discrepancy being a reduction in cooling by 5-10 W/m<sup>2</sup>. This may well be significant in terms of reduced overturning rates.

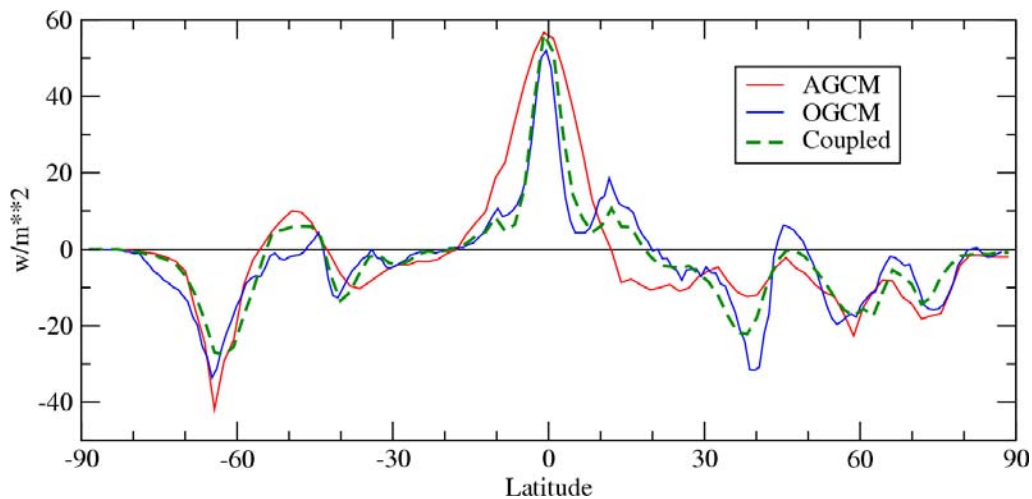


**Fig. 38** The surface heat flux for the coupled model, together with stand-alone AGCM and OGCM fluxes.

Overall, there have been some adjustments (often not very large) to the zonally averaged surface heat flux and water flux under coupled conditions. In the case of the heat flux, the largest changes are in the mid to high latitudes. In the case of freshwater flux, the largest changes are in the tropics, with the increase at about 10°S being consistent with the freshening seen in the surface salinity (Fig. 19) in the tropical Pacific Ocean.

### 8.14 Antarctic surface fluxes

The overturning in the Southern Ocean has been reduced in the Mk3.5 coupled model run relative to the Mk3.5 ocean spin-up (see Fig. 31). This contrasts with the increase that occurred in the Mk3.0 coupled model run. In Fig. 38 the zonally averaged surface water flux for the Mk3.0 and Mk3.5 model runs are displayed for the near Antarctic region (65°S to 85°S).

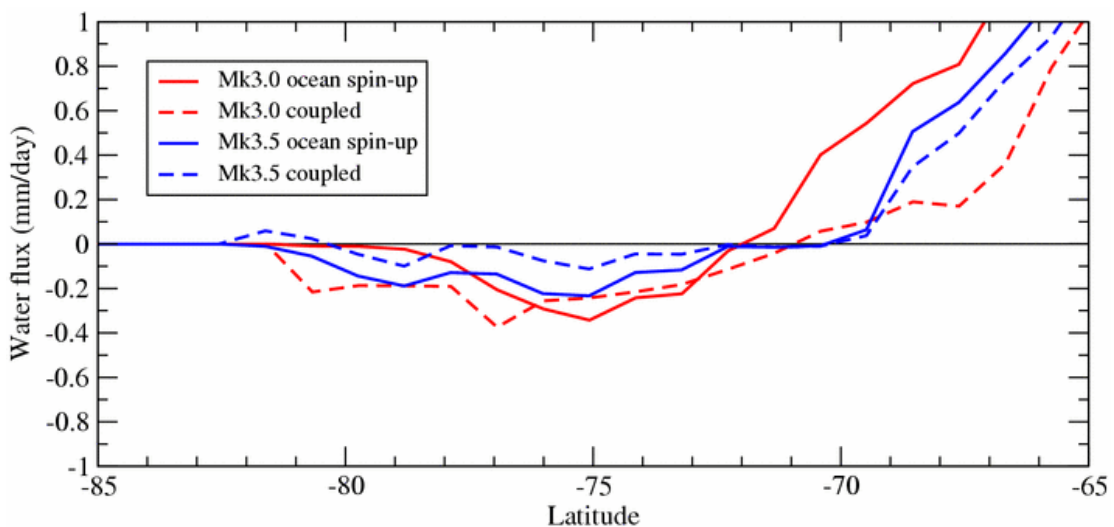


**Fig. 39** Antarctic zonal surface water flux from the Mk3.0 and Mk3.5 models.

In the Mk3.0 model runs, the water flux in the coupled run (years 71-80) has become more negative relative to the ocean spin-up case. (The Mk3.0 ocean spin-up was forced by relaxation

to Levitus). In the Mk3.5 model runs, the water flux has become less negative relative to the ocean spin-up. (The Mk3.5 ocean spin up was forced by AGCM fluxes plus relaxation to Levitus). Thus, in the Mk3.0 coupled run, there would be a tendency for more saline water, while in the Mk3.5 coupled run the Antarctic water would tend to become less saline. Thus, in the Mk3.5 run, the Antarctic water would tend to become less dense which would decrease the amount of overturning.

The reasons for the changed fresh water flux amounts in each coupled model run remains to be fully clarified. A preliminary examination is now presented. The fresh water flux is a combination of P-E, runoff, and contributions from sea-ice formation and melting. The volume of SH sea-ice and its coverage did not change significantly in the Mk3.5 coupled run (see subsection 9.7) and so changes to P-E and associated runoff might be responsible. In the model, precipitation over land (including Antarctica) leads to runoff which feeds directly into the oceans. The changes in zonally averaged runoff rates into the ocean (not shown) were most noticeable in the tropics, with very little change in mid to high latitudes. The change in zonally averaged ocean rainfall and evaporation between the Mk3.5 coupled run (years 101-140) and the AGCM spin-up is shown in Fig. 39. (The change in zonally averaged values for land and ocean together produced similar values.)

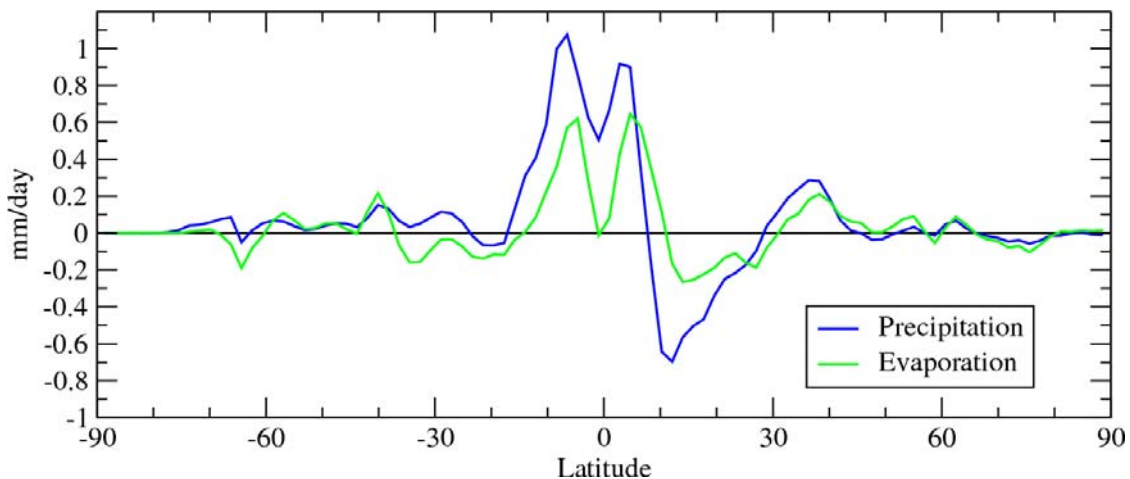


**Fig. 40 Mk3.5 ocean precipitation and evaporation: Coupled model – AGCM.**

The change in zonal precipitation and evaporation rates is quite small for the high latitudes in the NH. There are larger changes in the tropics, and in general there are changes of the same sign for both precipitation and evaporation. However, in the near Antarctic region (65°S to 85°S), there has been some increase in precipitation relative to evaporation. The ocean water flux has become less negative (leading to a decrease in surface salinity) in the Mk3.5 coupled model relative to spin-up (see Fig. 19) thus appears to be partly caused by increased precipitation. Around 60°S-65°S there has been a marked decrease in evaporation rate (without much change in precipitation) which would imply a decrease in salinity at those latitudes. Thus, both the changes to precipitation and evaporation rates in the Mk3.5 coupled model run in the Antarctic region tend to lead to less saline surface waters which in turn implies less dense surface water leading to reduced overturning rates.

In addition to water flux changes in the Antarctic region, changes to the surface heat flux following coupling would also affect the production of dense enough surface water leading to overturning. In Fig. 40, the zonally averaged surface heat flux for the Mk3.0 and Mk3.5 model

runs are displayed for the near Antarctic region (60°S to 85°S). In the Mk3.0 model runs, the heat flux in the coupled run (years 71-80) was more negative than in the ocean spin-up (relaxation to Levitus). On the other hand, in the Mk3.5 model runs, the heat flux in the coupled run became less negative relative to the ocean spin-up. (The Mk3.5 ocean spin up was forced by AGCM fluxes plus relaxation to Levitus). Thus in the Mk3.0 coupled run there was a tendency for enhanced cooling relative to spin-up, while in the Mk3.5 coupled run the Antarctic heat flux has become less negative (relative to spin up) and this would lead to less cold water being generated. A full analysis of the causes of the changes in surface heat flux upon coupling in both runs (Mk3.0 and Mk3.5) remains to be undertaken.

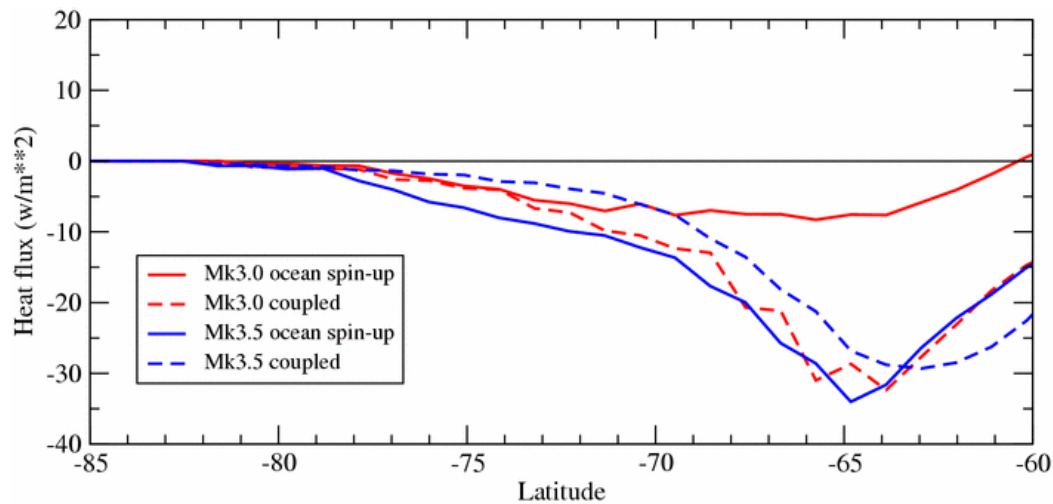


Fig. 41 Antarctic zonal net surface heat flux – Mk3.0 and Mk3.5 models.

## 8.15 A key coupled model response

In the near Antarctic region in the Mk3.5 coupled model, it has been shown that there have been some (small) changes to the zonally averaged surface heat and water fluxes generated by the AGCM when coupled compared to those in stand alone mode. The reduction in cooling and lessening of salinity enhancement *both* imply conditions less favourable to increases in density (especially locally). This is consistent with the reduced overturning in the Mk3.5 coupled model as seen in Fig. 31. The changes in the surface fluxes around the edge of the Antarctic do not appear to be related to changes in sea-ice cover and/or volume because the ice cover in the SH was very stable, and little changed between the AGCM spin-up state and the coupled state (see subsection 9.6 for a discussion of ice cover responses).

This underscores a major difficulty when modelling the coupled system. The above results imply that the coupled system needs to be able to generate surface heat and water fluxes at the surface, especially in polar regions, which are little different to those implied during the ocean model spin-up. Relatively small changes in surface fluxes appear to be able to suppress (or enhance as in the Mk3.0 coupled model) overturning in polar regions.

## 8.16 Concluding points

The results from the control run (subsections 9.1 to 9.15 above) are summarized by the following dot-points:

- A long control run (1300 years) has been undertaken.
- The model skill scores are, in general, better for Mk3.5 than for Mk3.0.
- The model showed very little drift in global mean SST.
- The global distribution of SST shows an improved “cold tongue” response in the tropical Pacific, but the excess coolness still evident there adversely affects Pacific rainfall patterns.
- The Nino3.4 SST responses (El Nino and La Nina events) are comparable to observations, but located too far to the west.
- The sea-ice in the coupled model is very similar to the uncoupled model, and has a realistic seasonal distribution.
- The Southern Ocean circulation in Mk3.5 is, in general, much improved over that in Mk3.0:
  - a. The Antarctic Circumpolar Current is much weaker, hence much more realistic
  - b. The wintertime mixed layers in the high latitude Southern Ocean are much shallower, again more realistic
  - c. The Antarctic overturning is much weaker, however in Mk3.5 this overturning appears too weak
  - d. The Antarctic surface fluxes, and their changes upon coupling, are found to play a key role in Southern Ocean coupled responses.
- The salinity distribution in the ocean is adversely affected by changes in rainfall patterns (especially in the tropical Pacific) and by the insufficient overturning in the Southern Ocean. The model becomes fresher at the surface and saltier in the deep oceans.

## 8.17 Data storage and access details

The model control run was 1300 years long. (See subsection 9.2 above for some additional details.) The Mk3.5 coupled model data for years 1-80 is stored on the CSIRO computer data store “Cherax” in sub-directories under “~gor079/C\_Mk3.5a.dir“. For years 81-1300, the data is stored under “~gor079/C\_Mk3.5d.dir“. Raw data in the form of NetCDF files both oceanic and atmospheric components of the model are stored in various subdirectories. Certain data files have subsequently been manipulated and refined by Mark Collier for general access. For the purposes of involvement of the CSIRO model in the 4<sup>th</sup> Assessment Report model intercomparison, the raw Mk3.5 model data was processed, validated and supplied according to the required standard set out in the document

[http://www-pcmdi.llnl.gov/ipcc/standard\\_output.html](http://www-pcmdi.llnl.gov/ipcc/standard_output.html)

The list of variables is not complete both in terms of what was requested by PCMDI<sup>4</sup> on behalf of IPCC but also in terms of what raw model data was available to process. Time resources did not allow for a complete set of the raw data to be processed, the Mk3.0 model submission was more complete in that regard. The report by Collier et al (2008) describes numerous features of the Mk3.0 submission and for many aspects the Mk3.5 submission was similar.

The principal method of obtaining CMIP3 Multi-Model data is to register with CMIP by going to the following web page

<https://esg.llnl.gov:8443/about/registration.do>

There are 2 other local methods for obtaining the processed Mk3.5 data. The first of these is to obtain an account on the CSIRO data store referred to as Cherax. The data is located under the account directory ~IPCC/data/mk3.5 following file and directory naming conventions set out by PCMDI. Please contact the CSIRO help desk to apply for an account on Cherax. The second method is to use OpenDap with the following address

[http://CMAR\\_mk3:ipcc4@hpsc.csiro.au/cgi-bin/OpenDAP/CMAR\\_mk3/nph-dods/mk3.5](http://CMAR_mk3:ipcc4@hpsc.csiro.au/cgi-bin/OpenDAP/CMAR_mk3/nph-dods/mk3.5)

This will allow you to browse datasets. However, send an email to [Martin.Dix@csiro.au](mailto:Martin.Dix@csiro.au) to apply for the access login and password to allow for downloading.

## 9 ACKNOWLEDGEMENTS

We would like to thank other members of the Earth Systems Modelling Program (part of CSIRO Atmospheric Research) who have contributed in various ways (including analysis of model results and data preparation) to the development of the Mk3.0 and then the Mk3.5 climate system models. Helpful comments on the manuscript were provided by Ian Smith. The Mk3.5 computations and analysis were performed on the NEC SX-6, TX-7 and Cray J90 computers at the CSIRO/Bureau of Meteorology Joint High Performance Computing and Communications Centre (Melbourne, Australia). The development of the Mk3 climate system model forms part of the CSIRO Climate Change Research Program, and has been funded in part by the Australian Greenhouse Office.

---

<sup>4</sup> <http://www-pcmdi.llnl.gov/about/index.php>

## 10 REFERENCES

- Alder, R.F., G.J. Huffman, A. Chang, R. Ferraro, P. Xie, J. Janowiak, B. Rudolf, U. Schneider, S. Curtis, D. Bolvin, A. Gruber, J. Susskind, P. Arkin, and E.J. Nelkin, 2003: The version-2 Global Precipitation Climatology Project (GPCP) monthly precipitation analysis (1979-present). *J. Hydrometeorol.*, **4**, 1147-1167.
- Bryan, K., 1984: Accelerating the convergence to equilibrium of ocean-climate models. *J. Phys. Oceanogr.*, **14**, 666-673.
- Collier, M. A., Dix, M. R., Hirst A. C., Davies, H. L., Elliott, T. I., Gordon, H. B., Morgan, P. J. L., O'Farrell, S. P., Rotstayn, L. D., and Watterson, I. G., 2008: IPCC Standard Output from the CSIRO Mk3.0 Climate System Model. CSIRO Marine and Atmospheric Research Paper No. 008. 466 pp.  
Available on-line at [http://www.cmar.csiro.au/e-print/open/2008/collierma\\_2008a.pdf](http://www.cmar.csiro.au/e-print/open/2008/collierma_2008a.pdf)
- CSIRO, and Bureau of Meteorology, 2007: Climate change in Australia. Technical Report, CSIRO, Melbourne. Available from [www.climatechangeinaustralia.gov.au](http://www.climatechangeinaustralia.gov.au) .
- Dengg, J., Böning, C., Ute, E., Redler, R., and Beckmann, A., 1999: Effects of an improved model representation of overflow water on the subpolar North Atlantic. International WOCE Newsletter 37. pp 10-15. Available via <http://woce.nodc.noaa.gov/wdiu/wocedocs/newsltr/news37/news37.pdf>
- Dümenil, L., Isele, K., Liebscher, H.J., Schröder, U., Schumacher, M., and Wilke, K., 1993: *Discharge data from 50 selected rivers for GCM validation*. Report No. 100, Max-Planck-Institut für Meteorologie, Hamburg.
- Gordon, H.B., 1981: A flux formulation of the spectral atmospheric equations suitable for use in long-term climate modelling. *Mon. Wea. Rev.*, **109**, 56-64.
- Gordon, H.B., Rotstayn, L.D., McGregor, J.L., Dix, M.R., Kowalczyk, E.A., O'Farrell, S.P., Waterman, L.J., Hirst, A.C., Wilson, S.G., Collier, M.A., Watterson, I.G. and Elliott, T.I., 2002: *The CSIRO Mk3 Climate System Model*. CSIRO Atmospheric Research Technical Paper No. 60. (Available on-line at [http://www.cmar.csiro.au/e-print/open/gordon\\_2002a.pdf](http://www.cmar.csiro.au/e-print/open/gordon_2002a.pdf) )
- Kraus, E.B., and Turner, J., 1967: A one dimensional model of the seasonal thermocline II. The general theory and its consequences. *Tellus*, **19**, 98–106.
- McGregor, J.L., 1993: Economical determination of departure points for semi-Lagrangian models. *Mon. Wea. Rev.*, **121**, 221-230.
- Mechoso, C.R., A.W. Roberston, N. Barth, M.K. Davey, P. Delecluse, P.R. Gent, S. Ineson, B. Kirtman, M. Latif, H. LeTreut, T. Nagai, J.D. Neelin, S.G.H. Philander, J. Polcher, P.S. Schopf, T. Stockdale, M.J. Suarez, L. Terray, O. Thual, and J.J. Tribbia, 1995: The seasonal cycle over the tropical Pacific in coupled ocean-atmosphere general circulation models. *Mon. Wea. Rev.*, **123**, 2825-2838.

- Meehl, G.A., P. Gent, J.M. Arblaster, B.L. Otto-Bliesner, E. Brady, and A. Craig, 2001: Factors that affect the amplitude of El Niño in global coupled climate models. *Climate Dyn.*, **17**, 515–526.
- Miller, J.R., Russell, G. L., and Caliri, G., 1994: Continental-scale river flow in climate models. *J. Climate*, **7**, 914-928.
- Monterey, G. and S. Levitus, 1997: Seasonal variability of mixed layer depth for the world ocean. NOAA Atlas NESDIS 14, U.S. Gov. Printing Office, Wash., D.C., 96 pp. 87 Figs
- O’Farrell, S.P., J.L. McGregor, L.D. Rotstayn, W.F. Budd, C. Zweck and R. Warner, 1997: Impact of transient increases in atmospheric CO<sub>2</sub> on the accumulation and mass balance of the Antarctic ice sheet. *Annals Glaciol.*, **25**, 137-144.
- O’Farrell, S.P., 1998: Investigation of the dynamic sea-ice component of a coupled atmosphere sea-ice general circulation model. *J. Geophys. Res.*, **103** (C8), 15751-15782.
- O’Farrell, S.P., and W.M. Connolley, 1998: Comparison of warming trends predicted over the next century around Antarctica from two coupled models. *Annals of Glaciology*, **27**, 576-582.
- Pacanowski, R.C., 1996: MOM2 Version 2.0: Documentation User's Guide and Reference Manual, GFDL Ocean Technical Report 3.2, 329 pps. (See [http://www.gfdl.noaa.gov/cms-filessystem-action/model\\_development/ocean/manual2.2.pdf](http://www.gfdl.noaa.gov/cms-filessystem-action/model_development/ocean/manual2.2.pdf))
- Pincus, R., C.P. Batstone, R.J. Patrick Hofmann, K.E. Taylor and P.J. Glecker, 2008: Evaluating the present-day simulation of clouds, precipitation, and radiation in climate models. *J. Geophys. Res.*, **113**, D14209, doi:10.1029/2007JD009334.
- Randall, D.A., R.A. Wood, S. Bony, R. Colman, T. Fichet, J. Fyfe, V. Kattsov, A. Pitman, J. Shukla, J. Srinivasan, R.J. Stouffer, A. Sumi and K.E. Taylor, 2007: Climate Models and Their Evaluation. In: *Climate Change 2007: The Physical Science Basis. Contribution of Working Group I to the Fourth Assessment Report of the Intergovernmental Panel on Climate Change* [Solomon, S., D. Qin, M. Manning, Z. Chen, M. Marquis, K.B. Averyt, M. Tignor and H.L. Miller (eds.)]. Cambridge University Press, Cambridge, United Kingdom and New York, NY, USA.
- Rotstayn, L. D., M. A. Collier, M. R. Dix, Y. Feng, H. B. Gordon, S. P. O’Farrell, I. N. Smith, J. Syktus. (2010). Improved simulation of Australian climate and ENSO-related climate variability in a GCM with an interactive aerosol treatment. *Int J. Climatol.*, doi: 10.1002/joc.1952.
- Sime, L.C., D.P. Stevens, K.J. Heywood and K.I.C. Oliver, 2006: A decomposition of the Atlantic Meridional Overturning. *J. Phys. Oceanogr.*, **36**, 2253-2270.
- Simmons, A.J., K.M. Willett, P.D. Jones, P.W. Thorne and D. Dee, 2009: Low-frequency variations in surface atmospheric humidity, temperature and precipitation: Inferences from reanalyses and monthly gridded observational datasets. *J. Geophys. Res.*, **114**. on-line.
- Smith, I., 2007: Global climate modelling within CSIRO: 1981 to 2006. *Aust. Met. Mag.*, **56**, 153-166.

Visbeck, M., J. Marshall, T. Haine and M. Spall, 1997: Specification of eddy transfer coefficients in coarse resolution ocean circulation models. *J. Phys. Oceanogr.*, **27**, 381-402.

Watterson, I.G., and M.R. Dix, 2005: Effective sensitivity and heat capacity in the response of climate models to greenhouse gas and aerosol forcings. *Quart. J. Roy. Met. Soc.*, **131**, 259-280.

Xie, P, and Arkin, P.A., 1997: Global precipitation. A 17-year monthly analysis based on gauge observations, satellite estimates and numerical model outputs. *Bull. Amer. Meteor. Soc.*, **78**, 2539-2558.

## 11 APPENDIX

### *River routing scheme for Mk3.5*

The Mk3.5 model has an upgraded river runoff scheme. The river runoff is directed, using the local topography for river direction, down to coastal points. The Mk3.0 model used instant transfer to the oceans, whereas the Mk3.5 model uses a time delay method with river flow being processed via “river-reservoirs” per model land point using flow velocities to adjacent grid points. This new river routing scheme is available as a model option “*newriver*”. It is currently only available for the T63 model.

Due to the complexity of the river system in reality, with the actual terrain not being adequately resolved by the T63 surface grid resolution, there is of necessity a pre-computation stage using a high resolution surface topography data set, together with manual intervention, to help define realistic surface flow directions for the river runoff on the model grid. In the model code, subroutine “*landrun*” is used to input precomputed values for the river routing scheme. Two of these quantities are the zonal and meridional topography gradients between grid points (*GradWE* and *GradSN*). In computing the directional flow of river runoff, it is found that there are land grid points which act as “troughs” due to the coarse nature of the T63 model resolution. A trough is a point at which any river flow will accumulate because there is only apparent inflow allowed to that point. (See below for more detail.) Thus there is an input of precomputed data indicating the (*i, j*) index for 310 apparent troughs (at T63 resolution). The river flow at a trough then has to be directed, in a physically based way using an atlas of topography and actual rivers, to nearby (downstream) grid points, and thus there is an input of precomputed downstream pointers for the flow from the 310 troughs. Also input is “*TopmnT63*” which is the minimum topography value per grid point. This is derived from the 1/8 degree topography data set used to determine the gradients between T63 grid boxes. The *TopmnT63* value is used to regulate the rate of flow from a trough to the trough downstream.

Runoff is added to a “river-reservoir” at each grid point. Any reservoir with  $> 0$  amounts of water has the transfer computed to adjacent grid points using the precomputed gradients West-East or South-North. These gradients, *GradWE* and *GradSN*, are derived as follows. Using a 1/8 degree topography data set, each T63 grid box has 15x15 topography “pixels”. In Fig. 41 below is a representation of the pixels of interest (shown by “**x**”) in computing the W-E gradient between two adjacent T63 grid boxes. The average height of the pixels denoted by “**x**” in the left (W) grid box is compared to the average height of the pixels in the right (E) grid box.

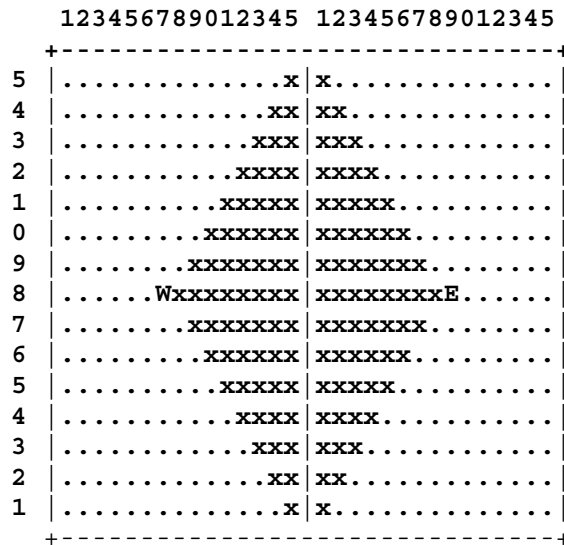


**Fig. 42 Topography pixels (x) used in W-E gradient calculation.**

The direction and rate of zonal flow between two grid boxes is determined by the gradient:

$$GradWE = (TaW - TaE) / (\Delta L \cos(\phi)) \quad 12.1$$

where

- $TaW$  = Average topographic height in W triangle
- $TaE$  = Average topographic height in E triangle
- $\Delta L$  = Grid length (equatorial)
- $\phi$  = Latitude

The same method applies in computing flow in the meridional direction. In Fig. 42 is a representation of the pixels of interest (shown by “x”) in computing the S-N gradient between 2 adjacent T63 grid boxes. The average height of the pixels denoted by “x” in the lower (S) grid box is compared to the average height of the pixels in the upper (N) grid box.

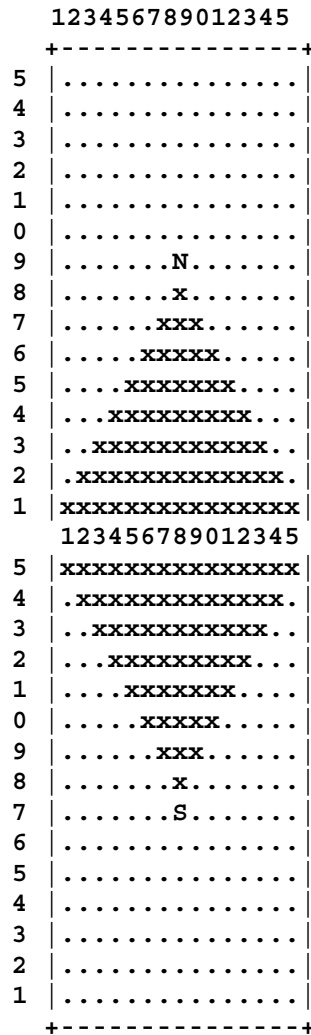


Fig. 43 Topography pixels (x) used in S-N gradient calculation.

The direction and rate of meridional flow between two grid boxes is determined by the gradient:

$$GradSN = (TaS - TaN) / \Delta L \quad 12.2$$

where

$TaS$  = Average topographic height in S triangle

$TaN$  = Average topographic height in N triangle

The topography gradients  $GradWE$  and  $GradSN$  are pre-computed as (m/m) and are input via subroutine "landrun". These are converted to flow velocities (m/sec) according to Miller et al. (1994):

$$vWE = 0.35 * sqrt(abs(GradWE) / 0.00005) \quad 12.3$$

$$vSN = 0.35 * \text{sqrt}(\text{abs}(\text{GradSN}) / 0.00005) \quad 12.4$$

These velocities are limited to a minimum of 0.15m/sec and a maximum of 5m/sec. The velocities are then converted (with scaling appropriate to T63 resolution) to a fraction of river-reservoir removed per model timestep:

$$fWE = (\Delta t / 15) * 0.0256 * \text{sign}(vWE, \text{GradWE}) \quad 12.5$$

$$fSN = (\Delta t / 15) * 0.0256 * \text{sign}(vSN, \text{GradSN}) \quad 12.6$$

Here  $\Delta t$  is the model time step in minutes – nominally 15 for the T63 model. The Fortran “*sign*” function is used to transfer the appropriate sign to the LHS values (see subroutine *landrun*). The fractions *fWE* and *fSN* are used to compute the transfer of river-reservoir values between adjacent grid squares. This is carried out in subroutine *newriv* using temporary river reservoir arrays “*resvr1*” and “*resvr2*” to carry out the (vectorised) transfer.

As mentioned above, when computing the directional flow from grid square to grid square, using flow between adjacent squares both zonally and meridionally, it is found that at the given resolution of the model (T63 in this case) there are grid squares that are effectively “troughs” with flow being able to enter but not escape. This happens mainly because at the model resolution, there is insufficient detailed topography resolved to be able Sahara desert. Other basins may contain lakes, but in many cases these basins have sufficient evaporation to remove water inflow. At the current model resolution, using the above method for determining downslope flow, it is found that there are about 310 (computed) troughs and basins. The river inflow (if any) into the troughs has to be taken care of. The troughs are assessed manually, using a world atlas, to determine where (unresolved) river flows would direct the river flow in reality. Directional pointers are created per trough, which are used in the model code to transfer river water from the trough to a non-adjacent grid square (downstream or to the nearby ocean point). The topographic basins are also given directional pointers to allow for any river inflow to escape and not accumulate indefinitely. A future refinement to this scheme would be to allow the river inflow into basins to effectively be put back into the grid wide soil moisture and thereby evaporate. This would be a representation of an inland river delta, an example of which is the Okavango delta in Botswana. Lake Eyre in South Australia is another example of a basin with a lake without an escape route for river water to the world oceans.

From now on we will use the word “trough” to indicate either a trough or a basin. The river flow from a trough “T” is directed to a non-adjacent grid square downstream “DS” which may be several (more than 1) grid points away in any direction. In the model code it was found useful to set up a pointer (single value) for the direction of flow from the trough “T” (see Fig. 43) that has 8 directions: either E(=1), NE(=2), N(=3), NW(=4), W(=5), SW(=6), S(=7), or SE(=8). The directions 2 = NE = North-Easterly, 4 = NW = North-Westerly, 6 = SW = South-Westerly, and 8 = SE = South-Easterly are used to imply directions that are not directly meridional or zonal, and thus can be approximate to capture sub-grid scale river valleys which allow for river flow to escape downstream, and thereby to other non-adjacent grid squares.

There are also regions in the world which are actually “basins”, with no escape route to the world oceans. Some basins are in arid parts of the world, e.g. parts of the Sahara desert.

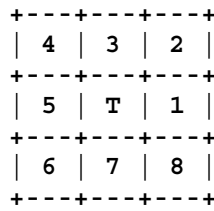


**Fig. 44 Schematic showing “pointer” locations at a trough point “T”. 1 = Easterly, 2 = North-Easterly, 3 = Northerly, etc.**

The above pointer is particularly useful for implementing the appropriate grid weighting for trough to trough transfers in the meridional direction, whilst allowing the relevant computer code to be readily vectorized on super-computers.

Using the  $(i, j)$  index of the grid point T (trough/basin) and the  $(ids, jds)$  index of the predetermined downstream grid square DS, a simple distance factor “*Distf*” is incorporated to reduced the transfer rate between troughs (relative to adjacent grid square transfer) due to the implied extra distance traveled:

$$Distf = sqrt( (i - ids)^2 + (j - jds)^2 ) \quad 12.7$$

In addition, the Great Lakes (North America) are treated explicitly (see below) and the *Distf* values for two troughs associated with the Niagara Falls and a downstream point are made larger ( $Distf = 10$ ) to help retard the river flow rates on the St Lawrence River at these points.

The distance factor is also modified to reflect the relative heights of the lowest point (1/8 degree topography pixel value) in the trough and in the DS point. The (pre-determined) minimum pixel height per grid square  $(i, j)$  is given by  $TopmnT63(i, j)$ . The difference in minimum pixels heights is then computed as

$$Topdiff = max( 10.0, TopmnT63(i, j) - TopmnT63(ids, jds) ) \quad 12.8$$

The flow rate downstream is made (weakly) dependent upon the *Topdiff* value (meters) by the factor

$$Tdl10 = log10 (Topdiff) \quad 12.9$$

It is found that *Tdl10* has values from 1 to just over 3. Thus *Distf* is replaced by a modified value given by  $Distf / Tdl10$ . This effectively increases the flow rate in regions of steep topography when transferring between troughs.

The river routing method then proceeds as follows. The water in the river-reservoirs is transferred between adjacent grid points (gradient flow) using the pre-computed fractional

values  $fWE$  and  $fSN$  appropriate to *adjacent* grid boxes. The direction of flow is accounted for. In addition, the change in grid size in the meridional direction (grid size weighting) also has to be included. River water will end up at ocean points by this process.

Next the river water arriving at the troughs “T” is moved to predefined downstream points “DS”. A flow rate “ $FR$ ”, for transfer between troughs, is first defined. For the T63 model we use  $FR = 0.001$ . This is an adjustable number which can be used to optimize the river flow rates. The trough river-reservoir water amount ( $Trw$ ) is then reduced by an amount given by

$$(FR / Distf) * (\Delta t / 15) * \max(0.0, Trw) \quad 12.10$$

This amount is transferred to the predetermined down-stream point using the computed pointer values, together with appropriate grid size weighting for meridional transfers. The use of the  $\max(\sim)$  function above relates to the treatment of the Great Lakes in which the river-reservoir value may be less than zero, and in this case the transfer of water from the troughs designated as representing the Great Lakes is inhibited until the lakes become overfull again. This is discussed in more detail below.

### The Great Lakes

Grid points which cover the Great Lakes (and some other large lakes in North America) are treated as water filled grid points in Mk3.5. This has been accomplished within the context of the Mk3.0 land-surface scheme. The water in the lake grid points is allowed to freeze and melt. It is noted here that land points have a soil model with six layers each having three prognostic variables: temperature, liquid water, and ice content. (See Mk3.0 Technical Report, Gordon et al. 2002). There is also a “puddle depth” (variable  $pmc$ ) for excess moisture held at the surface. These quantities are adapted for use in the (new) treatment of the Great Lakes in the Mk3.5 model code. The lakes are taken to be have unlimited water supply for evaporation (unlike land points), and the six lake levels are always saturated.

The grid points designated as lakes are defined in subroutine “*insoilveg*”. These grid points also defined to have saturation properties within the land surface scheme. The “fraction of ice”, as used for frozen land points, is used in lake points to show the fraction of frozen water per level. Further properties are defined for lake points in subroutine “*surfa*” and in a new subroutine “*surfa\_riv*”. The properties defined are for a completely wet surface, and the lakes treatment makes use of the “puddle depth” variable used for land points. For lake points the maximum puddle depth (“ $pmcmax$ ”) is set at 20mm (suitably large). For land points the puddle depth  $pmc$  is changed through rainfall addition, snow melt, and evaporation (subroutine “*surfb*”). The same occurs for the variable indicating “puddle depth” for lake points. However, in the case of lake grid points, if  $pmc$  is less than  $pmcmax$ , then  $pmc$  is reset to  $pmcmax$ , and the depth of water used to top up  $pmc$  is (subsequently) subtracted from the “river-reservoir” amount associated with lake points. On the other hand, if the  $pmc$  value for lakes exceeds  $pmcmax$ , then the excess is added to the lakes river-reservoir value at that grid point.

The depths of the 6 layers in the lakes are set to 3, 5, 7, 8, 8, and 8 m. These layers are used to compute changes in lake water temperature, with freezing being allowed (subroutine “*surfa\_riv*”) . In the case of lake points, any ice produced is required to be at the surface level(s). The water is also required to stable in the vertical (see second part of subroutine

“*surfa\_riv*”). The model results indicate that the temperature of the lowest level (6) for the lake points remains close to freezing throughout the year.

The grid points designated as representing the Great Lakes are shown schematically in Fig. 44. The T63 (i,j) index values are included along the top and on the RHS of the diagram respectively.

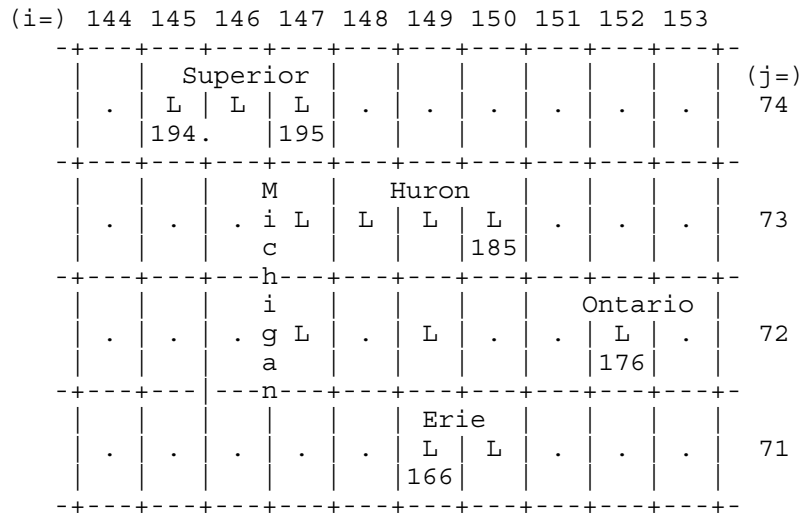


**Fig. 45 Schematic showing (i,j) locations of grid points representing the (T63) Great Lakes (L), together with (current model) “trough” indicator numbers.**

The topography “troughs” in the model (see discussion above) have specified numbers (0 to 309), and the trough numbers associated with the Great Lakes are also shown in the Fig. 44 (see model subroutine “*newriv*”). We thus have:

- Trough 194 = Lake Superior (West)
- Trough 195 = Lake Superior (East)
- Trough 185 = Lake Huron
- Trough 166 = Lake Erie (Niagara Falls between 166 and 176)
- Trough 176 = Lake Ontario

In computations involving the Great Lakes, all of the “L” grid points other than Lake Ontario above, are considered to be acting as one large lake when computing whether these combined lakes have a positive or negative average reservoir value. A positive average reservoir value indicates that there is downstream flow via the Niagara Falls to Lake Ontario. As mentioned above, there is an imposed slow transfer rate for any water between troughs 166 and 176 (Niagara Falls), and between 176 and downstream (St Lawrence River). On the other hand, if there is a negative average reservoir value, then flow downstream is not allowed until the lakes fill up to overflowing again.

Any water used to top up the Great Lakes *pmc* (“puddle depth”) to maximum (excluding L. Ontario) is then summed (with appropriate grid square area weighting) and subtracted from the river-reservoir amount at the L. Huron trough. The reservoir amounts in the 4 troughs (numbers 166, 185, 194, and 195) in the Great Lakes are then averaged so that these troughs have the same reservoir amount (positive or negative). Outflow from L. Erie to L. Ontario only occurs when there is a positive reservoir amount for the 4 troughs representing the (averaged) lakes.

There are two other sets of grid points in North America which are also treated as lakes. These are Lake Winnipeg (2 grid points with associated trough number 221), and the Baker Lakes (2 grid points with an associated trough number 273). As for the Great Lakes, the top up water for the *pmc* variable for these lakes is removed from the reservoir value at the trough.

### Modeled river flows

The AGCM, run with observed SSTs, has been used to assess the performance of the new river scheme. Given below in Table 3 is a comparison of observed and modeled outflows for the major rivers. The observations are taken from Dumenil et al. (1993). The top nine observed river outflow rates are shown, and also the outflow for the St. Lawrence River (associated with the Great Lakes treatment discussed above).

The river outflow values in the model reflect to a large degree the rainfall and associated runoff generated by the model, and thereby differences from observations. The model shows overly strong Amazon and Congo outflows. The outflow in the model for the grid point associated with the Parana River also includes the outflow from the R. Uruguay and this is partly the reason for the larger value shown in the model relative to the observations.

**Table 3. River outflows (1000m<sup>3</sup> sec<sup>-1</sup>)**

<b>River outflow</b>	<b>Observed</b>	<b>AGCM</b>
Amazon	155	242
Congo	40	101
Ganges + Bramaputra	34	40
Orinoco	31	24
Yangtze	29	13
Yenisey	18	21
Lena	17	11
Parana	16	41*
Baltic	15	10
---	---	---
St. Lawrence	8	12

\* Model grid point includes R. Uruguay outflow

There is a time delay imposed on the river flow by the new river routing scheme. This is illustrated Fig. 45. Here the Amazon River outflow per month is shown from the model (blue

line). There is a peak outflow in May/June, and a minimum in November. The 2 observations (shown by “Ob”) indicate a maximum in June and a minimum in October. On the other hand, for the old scheme with instantaneous river flow from land points to river outflow points, the outflow maximum occurs in February and the minimum in August (points ND on the graph). The new scheme is clearly giving a much better representation of the river outflow variations through the year.

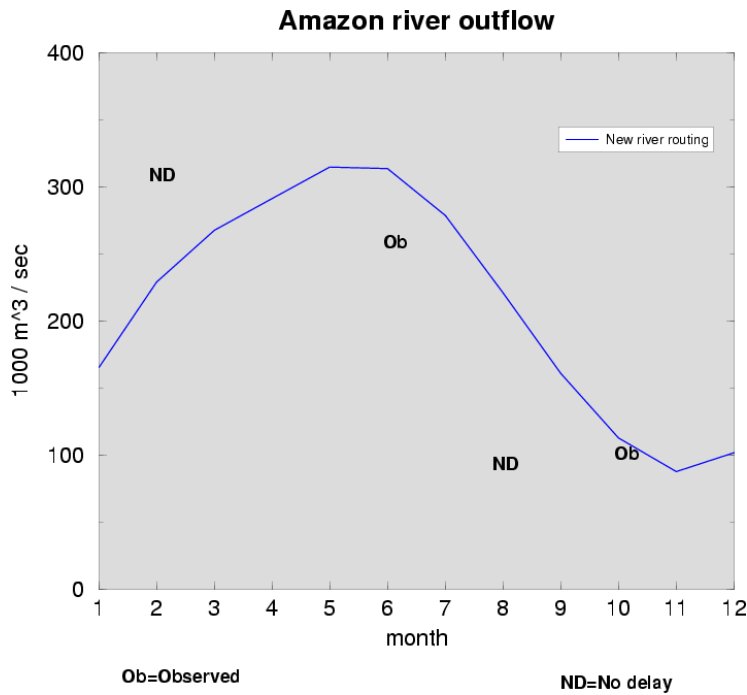


**Fig. 46 Amazon River monthly outflow rates.**

The new river routing scheme could be extended/improved in several ways. The modeled runoff into the river-reservoirs and downslope flow to the oceans does not yet take into account any direct evaporation from the rivers. Evaporation from rivers spreading through extensive flat marshland (e.g. the Nile flowing through marshes in Sudan) is not accounted for. There is also no account taken of human influences on river flow such as dams and irrigation. The inclusion of a representation of the Aswan Dam would clearly be beneficial to the modeled outflow rates for the Nile River into the Mediterranean (the current Nile outflow is too strong). The same applies to the outflow from the Murray River (Murray-Darling Basin) in Australia. The inclusion of a representation of the effect of inland river deltas (e.g. in the Okavango Basin) would be beneficial. The methodology used for the Great Lakes could be extended to other large lakes in the world. Lake Victoria and Lake Chad in Africa are examples. (In these particular lakes, freezing of lake water would be unlikely to occur.)

### Rivers with large volume outflows

Rivers such as the Amazon and Congo have large outflow rates, with a strong seasonal cycle. These strong outflow rates represent a very large input to the salinity tendency for the ocean model at those particular points. The modeled peak Amazon outflow of about  $0.3 \cdot 10^6 \text{ m}^3 / \text{sec}$  (0.3 Sv) is equivalent to a rainfall rate at the (AGCM) coastal grid point in

excess of 600 mm/day. The generated salinity tendency can lead to the formation of unwanted noise in a checker board pattern in salinity in the vicinity of the outflow. To help reduce this effect, outflows larger than a critical value are effectively smoothed over a “river delta” before use by the ocean model. This spreading out of river outflows is carried out in subroutine “*newriv*”, via subroutines “*spreadr*” and “*rivsprd*”. The river outflows are processed via two iterations. In the first iteration, any river outflows with an equivalent rainfall rate in excess of 60 mms/day have the excess spread over a 3x3 set of grid points (centred on the outflow grid point), with a bias towards more at the central grid point. The spreading is only done over the sea points within the 3x3 group of points. There is then a second iteration in which outflows with an equivalent rainfall rate that are still in excess of 40 mms/day are again spread over the local 3x3 group of points (sea points only). In this way the Amazon outflow may well end up being spread over a 4x4 group of points, in which the sea points represent some sort of river “delta”. The river delta data smoothing is carried out by the AGCM before the data is supplied to the OGCM as part of the salinity “P-E” forcing.

## Model development team

H.B. Gordon	( <a href="mailto:Hal.Gordon@dar.csiro.au">Hal.Gordon@dar.csiro.au</a> )	: Coupled model, spectral AGCM
S.P. O’Farrell	( <a href="mailto:Siobhan.OFarrell@dar.csiro.au">Siobhan.OFarrell@dar.csiro.au</a> )	: Sea-ice model and ocean model
M.A. Collier	( <a href="mailto:Mark.Collier@dar.csiro.au">Mark.Collier@dar.csiro.au</a> )	: Model data analysis
M.R. Dix	( <a href="mailto:Martin.Dix@dar.csiro.au">Martin.Dix@dar.csiro.au</a> )	: Radiation
L.D. Rotstayn	( <a href="mailto:Leon.Rotstayn@dar.csiro.au">Leon.Rotstayn@dar.csiro.au</a> )	: Cloud microphysics
E.A. Kowalczyk	( <a href="mailto:Eva.Kowalczyk@dar.csiro.au">Eva.Kowalczyk@dar.csiro.au</a> )	: Land surface model
A.C. Hirst	( <a href="mailto:Tony.Hirst@dar.csiro.au">Tony.Hirst@dar.csiro.au</a> )	: Ocean model
I.G. Watterson	( <a href="mailto:Ian.Watterson@csiro.au">Ian.Watterson@csiro.au</a> )	: Model evaluation





The Centre for Australian Weather and Climate Research is a partnership between CSIRO and the Bureau of Meteorology.